

An Extended Object PMB Filter with Zero-Inflated Poisson Model Using Belief Propagation

Xueqi Qiu, Yuxuan Xia, Hyowon Kim, Chaoqun Yang

Abstract

This paper presents an efficient implementation of the extended object Poisson multi-Bernoulli (PMB) filter under the zero-inflated Poisson (ZIP) object measurement model using particle belief propagation (BP). The ZIP measurement model separates a Bernoulli object detection event from the conditional Poisson generation of object measurements, enabling principled handling of empty measurement sets. Building upon the PMB mixture posterior, we present a factorized joint posterior over set of objects with object detection variables and a dual representation of data association using both object-oriented and measurement-oriented association variables. Notably, this representation replaces the implicit high-order global hypothesis constraint by local consistency factors, yielding a factor graph amenable to BP. In addition, we present a particle-based implementation, in which the Poisson intensity for undetected objects is analytic, whereas the single object densities of Bernoulli components for the detected objects are represented using particles. Simulation results demonstrate that the proposed method has superior performance than existing sampling-based implementations of extended object PMB filter with ZIP model in terms of both estimation accuracy and runtime.

Index Terms

Extended object tracking, multi-object tracking, Poisson point process, belief propagation

I. INTRODUCTION

Multi-object tracking (MOT) considers estimating the states of multiple objects from sequences of noisy sensor measurements [1]. High-resolution sensors, such as lidar and automotive radar, often produce multiple measurements from a single object. Tracking such objects is called extended object tracking (EOT), where the object state includes both kinematic and extent parameters [2]. In this paper, we focus on multiple EOT with an unknown and time-varying number of objects.

For EOT, the set of single object measurements is commonly modeled using an inhomogeneous Poisson point process (PPP) [3], where the number of measurements is Poisson distributed and the measurements are independently and identically distributed conditioned on the object state. Because of this, the PPP measurement model avoids explicit associations between measurements and reflection points on objects, thereby making it convenient to use in EOT.

The zero-inflated Poisson (ZIP) model augments the PPP with an explicit Bernoulli detection event. Under this model, an object is first detected with some probability, and only if it is detected, it then generates a Poisson set of measurements. Consequently, unlike the standard PPP model, the ZIP model can account separately for object missed detections and for the Poisson variability in the number of generated measurements. This separation is particularly beneficial for multiple EOT in scenarios with closely-spaced or partially occluded objects, since it provides a more flexible and interpretable measurement model. Both Poisson and ZIP measurement models have been used in many different multiple EOT algorithms, including, e.g., the multiple hypothesis tracker (MHT) [4], [5], the joint probabilistic data association filter [6], [7], and many filters based on random finite sets (RFS) [8]–[12].

For standard multi-object models with Poisson birth and the general measurement model that each object generates an independent set of measurements, the multi-object posterior is of the Poisson multi-Bernoulli mixture (PMBM) form [13], [14]. The PMBM density admits a compact representation of global hypotheses with probabilistic object existence encoded in each Bernoulli component, and it also enables measurement-driven track initiation by representing undetected objects as a PPP [15]. The PMBM filtering recursions have been derived for point objects [15], extended objects [11] and more general measurement models [13], [14]. The Poisson multi-Bernoulli (PMB) filter is an efficient approximation of the PMBM filter that approximates the PMBM posterior as a PMB [12], [16]. The extended object PMBM and PMB filters have been shown to achieve strong performance compared to many other multi-object filters [11], [12], [17].

A central challenge in multiple EOT is the data association problem, which needs to be efficiently addressed to keep the computational complexity of multiple EOT methods tractable. The most common solution is by enumerating data association hypotheses with high weights and pruning those with negligible weights. Approaches of this kind include the two-step method based on clustering and assignment (C&A) [10], [11] and sampling-based methods [18]. However, the performance of C&A-based methods often sharply drop in scenarios with objects moving in proximity, and sampling-based methods often have a high computational cost.

X. Qiu is with the Department of Computer Science, Durham University, Durham DH13LT, United Kingdom. Email: xueqi.qiu@durham.ac.uk. Y. Xia is with the School of Automation and Intelligent Sensing, Shanghai Jiao Tong University, Shanghai 200240, China. Email: yuxuan.xia@sjtu.edu.cn. H. Kim is with the Department of Electronics Engineering, Chungnam National University, Daejeon 34134, South Korea. Email: hyowon.kim@cnu.ac.kr. C. Yang is with the School of Automation, Southeast University, Nanjing 210096, China Email: ycq@seu.edu.cn

A more scalable approach that avoids explicit enumeration of data associations is to directly compute the marginal multi-object posterior density, where the data association uncertainties are marginalized out. This can be achieved by performing belief propagation (BP) on a factor graph representation of the joint posterior over data association variables and multi-object states [17], [19]. In particular, [17] shows that, for the extended object PMB filter, its particle BP-based implementation outperforms both C&A-based and sampling-based implementations in a challenging scenario with multiple objects moving in proximity.

However, the BP-based implementations in [17], [19] are developed for the PPP measurement model and do not explicitly model the object detection probability, while the C&A-based and sampling-based implementations in [11], [18] can handle the more general ZIP measurement model. The ZIP model makes it more challenging for BP because, when no measurements are generated, this event may result either from a missed detection under the Bernoulli detection mechanism or from an object being detected but still producing zero Poisson measurements. This ambiguity introduces an additional coupling in the joint posterior, leading to a high-order factor in the corresponding factor graph, which is not well suited for efficient BP.

An analytical BP implementation for the ZIP measurement model was proposed in [20] for the gamma Gaussian inverse-Wishart (GGIW) model and later extended to multi-sensor fusion in [21], but it has neglected the possibility that the Poisson detection branch of the ZIP model might still generate zero measurements. Furthermore, analytical GGIW implementations rely on clustering methods to enumerate data association hypotheses in computing the extrinsic messages for Bernoulli components, which can degrade performance in scenarios with closely-spaced objects. This has been improved in [22], where the intractable terms involved in computing the extrinsic messages are approximately computed using importance sampling. However, we find that the factorization of the joint posterior in [22, Eq. 10] is algebraically inconsistent with the introduced factors¹. An alternative factor graph formulation under the ZIP model is presented in [23], and the max-sum message passing is employed to compute the maximum a posteriori (MAP) data association. However, retaining only the MAP solution may result in degraded performance when data association uncertainty is high. Moreover, the corresponding factor for ZIP in the factor graph remains high-order in [23], making it unsuitable for efficient BP.

In light of the above discussion, there is a need for an efficient BP-based implementation of the extended object PMB filter under the ZIP measurement model that can well handle the coupling introduced by the ZIP model and avoid explicit enumeration of data association hypotheses. To this end, we present an efficient implementation of the extended object PMB filter under the ZIP measurement model using BP. We note that in this paper we focus on the estimation of the current object states, and the explicit estimation of object trajectories can be achieved by considering sets of trajectories [17], [24], [25].

The main contributions of this paper are summarized as follows:

- We present a joint factorized posterior for the extended object PMB update under the ZIP measurement model. Specifically, by introducing auxiliary object detection variables and a dual data association representation using both object-oriented and measurement-oriented association variables, we obtain a factor graph amenable to BP.
- We derive the corresponding message passing and belief calculation equations for the Bernoulli components.
- We develop a particle-based implementation of the proposed extended object PMB filter using BP.
- We compare the proposed method with existing sampling-based implementations [18] under the ZIP model. The results show superior performance of the proposed method in terms of both estimation accuracy and runtime.

The rest of the paper is organized as follows. In Section II, we present the standard multi-object models, the PMBM density and its PMB approximation on an augmented space with auxiliary variables, and the PMB filtering recursion. In Section III, we present the joint posterior representation for the PMB update under the ZIP measurement model, its factorization. In Section IV, we present the equations for performing loopy belief propagation on the factor graph representation of the joint posterior, and in Section V we present the particle-based implementation. In Section VI, we present the simulation results comparing the proposed method with existing methods. Finally, we conclude the paper in Section VII.

II. BACKGROUND

In this section, we first introduce the standard multi-object dynamic and measurement models with Poisson birth and ZIP object-generated measurements. Next, we present the PMBM density and its best PMB approximation on a space with auxiliary variables. Then, we present the PMB filtering recursion.

A. Multi-Object Models

The single object state $x_k \in \mathbb{R}^{d_x}$ at time step k contains information of the object, including e.g., its kinematic state and its extent state, which describes its shape and size. The set of object states at time step k is $\mathbf{x}_k = \{x_k^1, \dots, x_k^{n_k}\} \in \mathcal{F}(\mathbb{R}^{d_x})$, and the set of measurements at time step k is $\mathbf{z}_k = \{z_k^1, \dots, z_k^{m_k}\} \in \mathcal{F}(\mathbb{R}^{d_z})$. The sequence of measurement sets up to and including time k is denoted as $\mathbf{z}_{1:k}$.

1) *Dynamic model*: At time step k , new objects are born following a PPP with birth intensity $\lambda_k^B(x_k)$, independently of any existing objects. Each existing object x_{k-1} survives with probability $p_k^S(x_{k-1})$, and if it survives, it evolves according to the Markovian transition density $g_k(x_k|x_{k-1})$, independently of any other objects.

¹In particular, in the appendix of [22], Eqs. (B.19) and (B.22) do not reproduce the legacy-object no-association branch of Eq. (B.18).

2) *Measurement model*: The set \mathbf{z}_k of measurements is the union of object-generated measurements and clutter measurements. The set of clutter measurements is a PPP with Poisson intensity $\lambda_k^C(z_k) = \gamma_k^C \mu_k^C(z_k)$, where γ_k^C is the Poisson rate and $\mu_k^C(z_k)$ is the clutter spatial distribution.

A single object with state x_k generates an independent set \mathbf{w}_k of measurements with density $\ell_k(\mathbf{w}_k|x_k)$. In this work, we assume that \mathbf{w}_k is a ZIP process, and its set density is

$$\ell_k(\mathbf{w}_k|x_k) = \begin{cases} p_k^D(x_k)e^{-\gamma_k(x_k)} [\gamma_k(x_k)\ell_k(\cdot|x_k)]^{|\mathbf{w}_k|} & \mathbf{w}_k \neq \emptyset \\ 1 - p_k^D(x_k) + p_k^D(x_k)e^{-\gamma_k(x_k)} & \mathbf{w}_k = \emptyset, \end{cases} \quad (1)$$

where $p_k^D(x_k)$ denotes the detection probability. If object x_k is detected, it generates a Poisson set of measurements with rate $\gamma_k(x_k)$, and $\ell_k(\cdot|x_k)$ is the single measurement likelihood. The probability that object x_k generates at least one measurement is given by $1 - \ell_k(\emptyset|x_k) = p_k^D(x_k)(1 - e^{-\gamma_k(x_k)})$.

B. PMBM Density

Given a sequence of measurements $\mathbf{z}_{1:k'}$ up to and including time step $k' \in \{k-1, k\}$ and the multi-object models described in Section II-A, the exact multi-object density at time step k is of the PMBM form with [11]

$$f_{k|k'}(\mathbf{x}_k) = \sum_{\mathbf{x}_k^u \uplus \mathbf{x}_k^d = \mathbf{x}_k} f_{k|k'}^p(\mathbf{x}_k^u) f_{k|k'}^{mbm}(\mathbf{x}_k^d), \quad (2)$$

$$f_{k|k'}^p(\mathbf{x}_k^u) = \exp(-\langle \lambda_{k|k'}(\cdot), 1 \rangle) [\lambda_{k|k'}(\cdot)]^{\mathbf{x}_k^u}, \quad (3)$$

$$f_{k|k'}^{mbm}(\mathbf{x}_k^d) = \sum_{a \in \mathcal{A}_{k|k'}} w_{k|k'}^a \sum_{\uplus_{l=1}^{n_{k|k'}} \mathbf{x}_k^l = \mathbf{x}_k^d} \prod_{i=1}^{n_{k|k'}} f_{k|k'}^{i,a^i}(\mathbf{x}_k^i), \quad (4)$$

where the PPP $f_{k|k'}^p(\cdot)$ has intensity $\lambda_{k|k'}(\cdot)$, and it represents undetected objects that are hypothesized to exist but have not been detected, whereas the MBM $f_{k|k'}^{mbm}(\cdot)$ represents potential objects that have been detected at least once at some point up to time step k' .

The MBM in (4) has $n_{k|k'}$ Bernoulli components. For the i -th Bernoulli component, there are $h_{k|k'}^i$ local hypotheses, and its density under local hypothesis $a^i \in \{1, \dots, h_{k|k'}^i\}$ is

$$f_{k|k'}^{i,a^i}(\mathbf{x}_k^i) = \begin{cases} 1 - r_{k|k'}^{i,a^i} & \mathbf{x}_k^i = \emptyset \\ r_{k|k'}^{i,a^i} f_{k|k'}^{i,a^i}(x) & \mathbf{x}_k^i = \{x\} \\ 0 & \text{otherwise,} \end{cases} \quad (5)$$

where $r_{k|k'}^{i,a^i}$ is the probability of existence and $f_{k|k'}^{i,a^i}(\cdot)$ is the single object density conditioned on existence. The set $\mathcal{A}_{k|k'}$ contains all the global hypotheses [11]. Each MB component in (4) represents the density of the set \mathbf{x}_k^d of detected objects conditioned on a global hypothesis $a = (a^1, \dots, a^{n_{k|k}'}) \in \mathcal{A}_{k|k'}$, which selects a local hypothesis from each Bernoulli component. The weight of global hypothesis a satisfies

$$w_{k|k'}^a \propto \prod_{i=1}^{n_{k|k}'} w_{k|k'}^{i,a^i}, \quad (6)$$

where $w_{k|k'}^{i,a^i}$ is the weight of local hypothesis a^i for the i -th Bernoulli component, and normalization is required to ensure that $\sum_{a \in \mathcal{A}_{k|k'}} w_{k|k'}^a = 1$.

C. Poisson Multi-Bernoulli Approximation

The PMB is a special case of PMBM with a single MB. By augmenting the object space with auxiliary variables, the best PMB approximation can be obtained by minimizing the Kullback-Leibler divergence (KLD) [24]. To do so, we first augment the single object space with an auxiliary variable $u \in \mathbb{U}_{k|k'} = \{0, 1, \dots, n_{k|k}'\}$, such that $(u, x) \in \mathbb{U}_{k|k'} \times \mathbb{R}^{d_x}$. The auxiliary variable u can be interpreted as a track index: for $u = i \in \{1, \dots, n_{k|k}'\}$, x represents the state of the i -th potential object (also referred to as track in [16]), and for $u = 0$, x represents an undetected object. A set of objects equipped with track indices is then denoted as $\tilde{\mathbf{x}}_k \in \mathcal{F}(\mathbb{U}_{k|k'} \times \mathbb{R}^{d_x})$. Given $f_{k|k'}(\cdot)$ of the form (2), the density $f_{k|k'}(\cdot)$ on the space $\mathcal{F}(\mathbb{U}_{k|k'} \times \mathbb{R}^{d_x})$ is [24]

$$f_{k|k'}(\tilde{\mathbf{x}}_k) = f_{k|k'}^p(\tilde{\mathbf{Y}}_k) \sum_{a \in \mathcal{A}_{k|k}'} w_{k|k'}^a \prod_{i=1}^{n_{k|k}'} f_{k|k'}^{i,a^i}(\tilde{\mathbf{x}}_k^i) \quad (7)$$

where, for a given $\tilde{\mathbf{x}}_k, \tilde{\mathbf{y}}_k = \{(u, x) \in \tilde{\mathbf{x}}_k : u = 0\}$, $\tilde{\mathbf{x}}_k^i = \{(u, x) \in \tilde{\mathbf{x}}_k : u = i\}$, and

$$f_{k|k'}^p(\tilde{\mathbf{y}}_k) = \exp(-\langle \lambda_{k|k'}, 1 \rangle) [\lambda_{k|k'}(\cdot)]^{\tilde{\mathbf{y}}_k}, \quad (8a)$$

$$\lambda_{k|k'}(u, x) = \delta_0[u] \lambda_{k|k'}(x), \quad (8b)$$

$$f_{k|k'}^{i,a^i}(\tilde{\mathbf{x}}_k^i) = \begin{cases} 1 - r_{k|k'}^{i,a^i} & \tilde{\mathbf{x}}_k^i = \emptyset \\ \delta_i[u] r_{k|k'}^{i,a^i} f_{k|k'}^{i,a^i}(x) & \tilde{\mathbf{x}}_k^i = \{(u, x)\} \\ 0 & \text{otherwise.} \end{cases} \quad (8c)$$

We notice that the sum over sets in (2) disappears in (7) due to the use of auxiliary variables since now there is only one possible partition of $\tilde{\mathbf{x}}_k$ into $\tilde{\mathbf{y}}_k, \tilde{\mathbf{x}}_k^1, \dots, \tilde{\mathbf{x}}_k^{n_{k|k}'}$ that provides a non-zero density. If we integrate out the auxiliary variable u for each object, we recover the original PMBM density (2) [24]. We also note that in $\tilde{\mathbf{x}}_k$ there can be multiple objects with $u = 0$, but at most one object with $u = i \in \{1, \dots, n_{k|k}'\}$, for a non-zero density of (7).

Given a PMBM density $f_{k|k'}(\cdot)$ of the form (7), the PMB density that minimizes the KLD from $f_{k|k'}(\cdot)$ has closed form and is given by [24, Prop. 2]

$$f_{k|k'}^{pmb}(\tilde{\mathbf{x}}_k) = f_{k|k'}^p(\tilde{\mathbf{y}}_k) \prod_{i=1}^{n_{k|k}'} f_{k|k'}^i(\tilde{\mathbf{x}}_k^i), \quad (9a)$$

$$f_{k|k'}^i(\tilde{\mathbf{x}}) = \begin{cases} 1 - r_{k|k'}^i & \tilde{\mathbf{x}} = \emptyset \\ \delta_i[u] r_{k|k'}^i f_{k|k'}^i(x) & \tilde{\mathbf{x}} = \{(u, x)\} \\ 0 & \text{otherwise,} \end{cases} \quad (9b)$$

$$r_{k|k'}^i = \sum_{a^i=1}^{h_{k|k'}^i} \bar{w}_{k|k'}^{i,a^i} r_{k|k'}^{i,a^i}, \quad (9c)$$

$$f_{k|k'}^i(x) = \frac{\sum_{a^i=1}^{h_{k|k'}^i} \bar{w}_{k|k'}^{i,a^i} r_{k|k'}^{i,a^i} f_{k|k'}^{i,a^i}(x)}{r_{k|k'}^i}, \quad (9d)$$

$$\bar{w}_{k|k'}^{i,a^i} = \sum_{b \in \mathcal{A}_{k|k'}^i : b^i = a^i} w_{k|k'}^b. \quad (9e)$$

If we integrate out the auxiliary variables in (9), we obtain the PMB density without auxiliary variables [24]

$$f_{k|k'}^{pmb}(\mathbf{x}_k) = \sum_{\uplus_{l=1}^{n_{k|k}'} \mathbf{x}^l \uplus \mathbf{y} = \mathbf{x}_k} f_{k|k'}^p(\mathbf{y}) \prod_{i=1}^{n_{k|k}'} f_{k|k'}^i(\mathbf{x}^i) \quad (10)$$

where the i -th Bernoulli component $f_{k|k'}^i(\mathbf{x}^i)$ is parameterized by $r_{k|k'}^i$ in (9c) and $f_{k|k'}^i(x)$ in (9d).

D. Poisson Multi-Bernoulli Filtering

We first define the set of global hypotheses for extended objects. We refer to measurement \mathbf{z}_k^j using the pair (k, j) , and the set of all such pairs at time step k is denoted \mathcal{M}_k . We also let $\mathcal{M}_k^{i,a^i} \subseteq \mathcal{M}_k$ be the set of index pairs associated to local hypothesis a^i of the i -th Bernoulli component. Then, the set of all feasible global hypotheses is

$$\mathcal{A}_{k|k} = \left\{ (a^1, \dots, a^{n_{k|k}}) : a^i \in \{1, \dots, h_{k|k}^i\} \forall i, \biguplus_{i=1}^{n_{k|k}} \mathcal{M}_k^{i,a^i} = \mathcal{M}_k \right\}, \quad (11)$$

where the constructions of \mathcal{M}_k^{i,a^i} will be given in Lemma 2. We consider the PMB update, where each measurement creates a new Bernoulli component [12], instead of each non-empty subset of measurements creating a new Bernoulli component, as in [11].

Lemma 1. *Given the PMB filtering density at time $k-1$ of the form (10), the predicted density at time k is a PMB of the form (10), with $n_{k|k} = n_{k|k-1}$,*

$$\lambda_{k|k-1}(x) = \lambda_k^B(x) + \langle \lambda_{k-1|k-1}, g_k(x|\cdot) p^S(\cdot) \rangle, \quad (12a)$$

$$r_{k|k-1}^i = r_{k-1|k-1}^i \langle f_{k-1|k-1}^i, p^S \rangle, \quad (12b)$$

$$f_{k-1|k-1}^i(x) = \frac{\langle f_{k-1|k-1}^i, g_k(x|\cdot) p^S(\cdot) \rangle}{\langle f_{k-1|k-1}^i, p^S \rangle}. \quad (12c)$$

Lemma 2. Given the PMB predicted density at time step k of the form (10) and measurements $\mathbf{z}_k = \{z_k^1, \dots, z_k^{m_k}\}$, the updated density is a PMBM of the form (2), with

$$n_{k|k} = n_{k|k-1} + m_k, \quad (13)$$

$$\mathcal{M}_k = \{(k, j) \mid j \in \{1, \dots, m_k\}\}, \quad (14)$$

$$\lambda_{k|k}(x) = \ell_k(\emptyset|x)\lambda_{k|k-1}(x). \quad (15)$$

The i -th existing Bernoulli component, $i \in \{1, \dots, n_{k|k-1}\}$, has $h_{k|k}^i = 2^{m_k}$ local hypotheses, either corresponding to a misdetection or an update using a non-empty subset of \mathbf{z}_k . For a misdetection hypothesis, we have $\mathcal{M}_k^{i,1} = \emptyset$, and

$$\ell_{k|k}^{i,1,0} = \left\langle f_{k|k-1}^i, \ell_k(\emptyset|\cdot) \right\rangle, \quad (16a)$$

$$w_{k|k}^{i,1} = 1 - r_{k|k-1}^i + r_{k|k-1}^i \ell_{k|k}^{i,1,0}, \quad (16b)$$

$$r_{k|k}^{i,1} = \frac{r_{k|k-1}^i \ell_{k|k}^{i,1,0}}{1 - r_{k|k-1}^i + r_{k|k-1}^i \ell_{k|k}^{i,1,0}}, \quad (16c)$$

$$f_{k|k}^{i,1}(x) = \frac{\ell_k(\emptyset|x) f_{k|k-1}^i(x)}{\ell_{k|k}^{i,1,0}}. \quad (16d)$$

Let $\mathbf{w}_k^1, \dots, \mathbf{w}_k^{2^{m_k}-1}$ be the non-empty subsets of \mathbf{z}_k . For the i -th Bernoulli component $i \in \{1, \dots, n_{k|k-1}\}$, the local hypothesis generated by a set \mathbf{w}_k^j of measurements has index $a^i = 1 + j$ with $j \in \{1, \dots, 2^{m_k} - 1\}$, and

$$\mathcal{M}_k^{i,a^i} = \{(k, p) : z_k^p \in \mathbf{w}_k^j\}, \quad (17a)$$

$$\ell_{k|k}^{i,a^i,j} = \left\langle f_{k|k-1}^i, \ell_k(\mathbf{w}_k^j|\cdot) \right\rangle, \quad (17b)$$

$$w_{k|k}^{i,a^i} = r_{k|k-1}^i \ell_{k|k}^{i,a^i,j}, \quad (17c)$$

$$r_{k|k}^{i,a^i} = 1, \quad (17d)$$

$$f_{k|k}^{i,a^i}(x) = \frac{\ell_k(\mathbf{w}_k^j|x) f_{k|k-1}^i(x)}{\ell_{k|k}^{i,a^i,j}}. \quad (17e)$$

Each new Bernoulli component has a different number of local hypotheses, each created by a subset of \mathbf{z}_k . The set of subsets of measurements associated to the i -th new Bernoulli component ($i \in \{1, \dots, m_k\}$) can be recursively built as [12]

$$\mathcal{S}_i = \{\{z_k^i\}\} \cup \left(\bigcup_{\mathbf{w} \in \bigcup_{j=1}^{i-1} \mathcal{S}_j} \{\{z_k^i\} \cup \mathbf{w}\} \right), \quad (18)$$

with $\mathcal{S}_1 = \{\{z_k^1\}\}$. This implies that the i -th new Bernoulli component must contain the local hypothesis created by the single measurement z_k^i and cannot be associated with measurements with index larger than i . Further, we let $\mathbf{w}_k^{i,\iota} \in \mathcal{S}_i$ denote the ι -th non-empty subset of measurements associated to the i -th new Bernoulli component, with $i = n_{k|k-1} + j$, $j \in \{1, \dots, m_k\}$, $\iota \in \{1, \dots, 2^{j-1}\}$. The i -th new Bernoulli component has $h_{k|k}^i = 2^{j-1} + 1$ local hypotheses. The case corresponding to non-existence is given by

$$\mathcal{M}_k^{i,1} = \emptyset, \quad w_{k|k}^{i,1} = 1, \quad r_{k|k}^{i,1} = 0, \quad (19)$$

and the others ($a^i = \iota + 1, \iota \in \{1, \dots, 2^{j-1}\}$), corresponding to detection with $\mathbf{w}_k^{i,\iota}$, are given by

$$\mathcal{M}_k^{i,a^i} = \{(k, p) : z_k^p \in \mathbf{w}_k^{i,\iota}\}, \quad (20a)$$

$$\ell_{k|k}^{i,\iota} = \left\langle \lambda_{k|k-1}, \ell_k(\mathbf{w}_k^{i,\iota}|\cdot) \right\rangle, \quad (20b)$$

$$w_{k|k}^{i,a^i} = \delta_1 \left[\|\mathbf{w}_k^{i,\iota}\| \right] \lambda_k^C(z_k^j) + \ell_{k|k}^{i,\iota}, \quad (20c)$$

$$r_{k|k}^{i,a^i} = \frac{\ell_{k|k}^{i,\iota}}{w_{k|k}^{i,a^i}}, \quad (20d)$$

$$f_{k|k}^{i,a^i}(x) = \frac{\ell_k(\mathbf{w}_k^{i,\iota}|x) \lambda_{k|k-1}(x)}{\ell_{k|k}^{i,\iota}}. \quad (20e)$$

In (20), under the local hypothesis with $\mathbf{w}_k^{i,\iota} = \{z_k^j\}$, the Bernoulli set density accounts for the possibility that the measurement z_k^j is either clutter or generated by a newly detected object. If $|\mathbf{w}_k^{i,\iota}| > 1$, the local hypothesis corresponds to an object with existence probability one.

III. JOINT POSTERIOR AND ITS FACTORIZATION

In this section, we first present the joint posterior of the set of objects and global hypothesis. Then, we describe how to factorize this joint posterior for the ZIP measurement model, making it amenable to message passing.

A. Joint Posterior of Set of Objects and Global Hypothesis

We define the joint posterior of the set of objects $\tilde{\mathbf{x}}_k$ and global hypothesis a on the space $\mathcal{F}(\mathbb{U}_{k|k} \times \mathbb{R}^{d_x}) \times \mathcal{A}_{k|k}$ as

$$f_{k|k}(\tilde{\mathbf{x}}_k, a) = f_{k|k}^p(\tilde{\mathbf{x}}_k^u) w_{k|k}^a \prod_{i=1}^{n_{k|k}} f_{k|k}^{i,a^i}(\tilde{\mathbf{x}}_k^i) \propto f_{k|k}^p(\tilde{\mathbf{x}}_k^u) \prod_{i=1}^{n_{k|k}} w_{k|k}^{i,a^i} f_{k|k}^{i,a^i}(\tilde{\mathbf{x}}_k^i) \triangleq f_{k|k}^p(\tilde{\mathbf{x}}_k^u) \prod_{i=1}^{n_{k|k}} g_{k|k}^{i,a^i}(\tilde{\mathbf{x}}_k^i), \quad (21)$$

where $g_{k|k}^{i,a^i}(\cdot)$ correspond to unnormalized Bernoulli densities and can be computed as follows according to Lemma 2. Specifically, we have that, for missed detection hypotheses, with $i \in \{1, \dots, n_{k|k-1}\}$,

$$g_{k|k}^{i,1}(\tilde{\mathbf{x}}_k^i) = \begin{cases} \delta_i[u] r_{k|k-1}^i \ell_k(\emptyset|x) f_{k|k-1}^i(x) & \tilde{\mathbf{x}}_k^i = \{(u, x)\} \\ 1 - r_{k|k-1}^i & \tilde{\mathbf{x}}_k^i = \emptyset \\ 0 & \text{otherwise,} \end{cases} \quad (22)$$

and for detection hypotheses, with $a^i = 1 + j$, where $j \in \{1, \dots, 2^{m_k} - 1\}$,

$$g_{k|k}^{i,a^i}(\tilde{\mathbf{x}}_k^i) = \begin{cases} \delta_i[u] r_{k|k-1}^i \ell_k(\mathbf{w}_k^j|x) f_{k|k-1}^i(x) & \tilde{\mathbf{x}}_k^i = \{(u, x)\} \\ 0 & \text{otherwise.} \end{cases} \quad (23)$$

For the non-existence hypotheses for new Bernoulli components, with $i = n_{k|k-1} + j$, $j \in \{1, \dots, m_k\}$,

$$g_{k|k}^{i,1}(\tilde{\mathbf{x}}_k^i) = \begin{cases} 1 & \tilde{\mathbf{x}}_k^i = \emptyset \\ 0 & \text{otherwise,} \end{cases} \quad (24)$$

and for the existence hypotheses for new Bernoulli components, with $a^i = \iota + 1$, $\iota \in \{1, \dots, 2^{j-1}\}$

$$g_{k|k}^{i,a^i}(\tilde{\mathbf{x}}_k^i) = \begin{cases} \delta_i[u] \ell_k(\mathbf{w}_k^{i,\iota}|x) \lambda_{k|k-1}(x) & \tilde{\mathbf{x}}_k^i = \{(u, x)\} \\ \delta_1 \left[\left[\mathbf{w}_k^{i,\iota} \right] \lambda_k^C(z^j) \right] & \tilde{\mathbf{x}}_k^i = \emptyset \\ 0 & \text{otherwise.} \end{cases} \quad (25)$$

It can be observed that the joint posterior of the set of objects and the global hypothesis in (21) already admits a factorized form. Nevertheless, this form is not directly amenable to BP, since the global hypothesis $a \in \mathcal{A}_{k|k}$ is subject to the constraint in (11), which acts as an implicit high-order factor that couples the local hypotheses globally, thereby preventing a convenient decomposition into low-order factors for efficient BP.

B. Joint Posterior Factorization with Auxiliary Variables

To make the posterior more amenable to message passing, we first introduce binary object detection variables and dual representations of object-oriented and measurement-oriented data association variables in order to expose the latent structure of the PMB update with ZIP measurements. Specifically, for the i -th existing Bernoulli component, $i \in \{1, \dots, n_{k|k-1}\}$, we first introduce a binary object detection variable $D_k^i \in \{0, 1\}$, where $D_k^i = 1$ indicates that the object is detected at time step k (and generates a Poisson number $\gamma_k(\cdot)$ of measurements which can still be zero) while $D_k^i = 0$ indicates a missed detection that corresponds to the Bernoulli non-detection branch. Note that we do not need to introduce D_k^i for new Bernoulli components that represent newly detected objects. Then, we have

$$\ell_k^D(\mathbf{w}_k, D_k^i | \tilde{\mathbf{x}}_k^i) = \ell_k(\mathbf{w}_k | \tilde{\mathbf{x}}_k^i, D_k^i) f_k^{D,i}(D_k^i | \tilde{\mathbf{x}}_k^i), \quad (26)$$

where

$$f_k^{D,i}(D_k^i | \tilde{\mathbf{x}}_k^i) = \begin{cases} \delta_i[u] p_k^D(x) e^{-\gamma_k(x)} & \tilde{\mathbf{x}}_k^i = \{(u, x)\}, D_k^i = 1 \\ \delta_i[u] (1 - p_k^D(x)) & \tilde{\mathbf{x}}_k^i = \{(u, x)\}, D_k^i = 0 \\ 1 & \tilde{\mathbf{x}}_k^i = \emptyset, D_k^i = 0 \\ 0 & \text{otherwise,} \end{cases} \quad (27)$$

$$\ell_k(\mathbf{w}_k | \tilde{\mathbf{x}}_k^i = \{(u, x)\}, D_k^i) = \begin{cases} \delta_i[u] [\gamma_k(x) \ell_k(\cdot|x)]^{\mathbf{w}_k} & D_k^i = 1 \\ \delta_i[u] & D_k^i = 0, \mathbf{w}_k = \emptyset \\ 0 & \text{otherwise,} \end{cases} \quad (28)$$

$$\ell_k(\mathbf{w}_k | \tilde{\mathbf{x}}_k^i = \emptyset, D_k^i) = \begin{cases} 1 & D_k^i = 0, \mathbf{w}_k = \emptyset \\ 0 & \text{otherwise.} \end{cases} \quad (29)$$

If we marginalize D_k^i from (26), we recover the original ZIP measurement set density. By separating the Bernoulli detection event from the conditional Poisson measurements, we obtain a more explicit factorized representation (26).

We proceed to describe how to decompose the high-order factor introduced by the global association hypothesis constraint $a \in \mathcal{A}_{k|k}$ into a collection of lower-order factors suitable for BP. To do so, we introduce a dual representation of the data association, one object-oriented and one measurement-oriented. Although redundant, both representations are equivalent, in the sense that each admissible realization of either representation under the imposed constraints uniquely determines a global hypothesis. This redundancy allows the original global hypothesis constraint in (11) to be replaced by local consistency factors.

We first introduce the object-oriented association variables $\alpha_k = [(\alpha_k^1)^T, \dots, (\alpha_k^{n_k|k})^T]^T$, where

$$\alpha_k^i = \begin{cases} [\alpha_k^{i,1}, \dots, \alpha_k^{i,m_k}]^T & i \in \{1, \dots, n_{k|k-1}\} \\ [\alpha_k^{i,1}, \dots, \alpha_k^{i,j}]^T & i = n_{k|k-1} + j, j \in \{1, \dots, m_k\}, \end{cases} \quad (30)$$

with $\alpha_k^{i,j} \in \{0, 1\}$, and $\alpha_k^{i,j} = 1$ if and only if the j -th measurement z_k^j is associated with the i -th Bernoulli component. Note that the object-oriented association vector corresponding to the j -th new Bernoulli component has length j . This follows directly from the local hypothesis structure of new Bernoulli components described in Lemma 2.

In addition, according to the conditional measurement set density (26), if the potential object corresponding to the i -th Bernoulli component is not detected, then no measurement can be associated with it. To encode this relation, we introduce the binary factor

$$\Phi_k^{i,j} (D_k^i, \alpha_k^{i,j}) = \begin{cases} 1 & D_k^i = 1 \text{ or } \alpha_k^{i,j} = 0 \\ 0 & \text{otherwise,} \end{cases} \quad (31)$$

for $i \in \{1, \dots, n_{k|k-1}\}$ and $j \in \{1, \dots, m_k\}$. The product of these factors over index j ensures that no measurement can be associated with the i -th Bernoulli component when $D_k^i = 0$, while the case with $D_k^i = 1$ and all-zero $\alpha_k^{i,j}$ is still allowed, which represents that the corresponding object is detected but generates zero measurements.

We proceed to rewrite the unnormalized Bernoulli densities $g_k^{i,\alpha^i}(\cdot)$ using the object-oriented association variables α_k and binary detection variables $D_k^{1:n_k|k-1} = [D_k^1, \dots, D_k^{n_k|k-1}]^T$, leveraging the factorization of the conditional Poisson measurement set density (26). Specifically, for the i -th Bernoulli component with $i \in \{1, \dots, n_{k|k-1}\}$, we have

$$g_k^{D,i,\alpha^i}(\tilde{\mathbf{x}}_k^i, D_k^i) = f_k^{D,i}(D_k^i | \tilde{\mathbf{x}}_k^i) \underline{f}_{k|k-1}^i(\tilde{\mathbf{x}}_k^i) \prod_{j=1}^{m_k} \Phi_k^{i,j}(D_k^i, \alpha_k^{i,j}) \underline{s}_k^i(\tilde{\mathbf{x}}_k^i, \alpha_k^{i,j}; z_k^j), \quad (32)$$

and for $i = n_{k|k-1} + j, j \in \{1, \dots, m_k\}$,

$$g_k^{i,\alpha^i}(\tilde{\mathbf{x}}_k^i) = \bar{f}_{k|k-1}^i(\tilde{\mathbf{x}}_k^i) \bar{s}_k^i(\tilde{\mathbf{x}}_k^i, \alpha_k^{i,j}; z_k^j) \prod_{l=1}^{j-1} \underline{s}_k^i(\tilde{\mathbf{x}}_k^i, \alpha_k^{i,l}; z_k^l). \quad (33)$$

In (32) and (33), the local hypothesis a^i of the i -th Bernoulli component is now represented explicitly by the corresponding object-oriented association variable α_k^i (30), which provides an equivalent description of the measurement subset associated with that component. In addition, the new factors are

$$\underline{f}_{k|k-1}^i(\tilde{\mathbf{x}}_k^i) = \begin{cases} \delta_i[u] r_{k|k-1}^i f_{k|k-1}^i(x) & \tilde{\mathbf{x}}_k^i = \{(u, x)\} \\ 1 - r_{k|k-1}^i & \tilde{\mathbf{x}}_k^i = \emptyset \\ 0 & \text{otherwise,} \end{cases} \quad (34)$$

$$\bar{f}_{k|k-1}^i(\tilde{\mathbf{x}}_k^i) = \begin{cases} \delta_i[u] p_k^D(x) e^{-\gamma_k(x)} \lambda_{k|k-1}(x) & \tilde{\mathbf{x}}_k^i = \{(u, x)\} \\ 1 & \tilde{\mathbf{x}}_k^i = \emptyset \\ 0 & \text{otherwise,} \end{cases} \quad (35)$$

$$\underline{s}_k^i(\tilde{\mathbf{x}}_k^i, \alpha_k^{i,j}; z_k^j) = \begin{cases} \delta_i[u] \gamma_k(x) \ell_k(z_k^j | x) & \tilde{\mathbf{x}}_k^i = \{(u, x)\}, \alpha_k^{i,j} = 1 \\ 1 & \alpha_k^{i,j} = 0 \\ 0 & \text{otherwise,} \end{cases} \quad (36)$$

$$\bar{s}_k^i(\tilde{\mathbf{x}}_k^i, \alpha_k^{i,j}; z_k^j) = \begin{cases} \delta_i[u] \gamma_k(x) \ell_k(z_k^j | x) & \tilde{\mathbf{x}}_k^i = \{(u, x)\}, \alpha_k^{i,j} = 1 \\ \lambda_k^C(z_k^j) & \tilde{\mathbf{x}}_k^i = \emptyset, \alpha_k^{i,j} = 1 \\ 1 & \tilde{\mathbf{x}}_k^i = \emptyset, \alpha_k^{i,j} = 0 \\ 0 & \text{otherwise.} \end{cases} \quad (37)$$

In the above, the factors (34) and (35) represent the predicted and prior information for existing and newly detected objects, respectively, without being associated with any measurements, whereas the factors (36) and (37) represent the local likelihood of associating a particular measurement with its corresponding Bernoulli component for existing and newly detected objects, respectively.

Next, we introduce the measurement-oriented association variables $\beta_k = [\beta_k^1, \dots, \beta_k^{m_k}]^T$, where the j -th element $\beta_k^j = i$, $j \in \{1, \dots, m_k\}$, if and only if the j -th measurement z_k^j is associated with the i -th Bernoulli component. According to the local hypothesis structure for new Bernoulli components described in Lemma 2, the j -th measurement z_k^j cannot be associated with a new Bernoulli component, whose index is smaller than $n_{k|k-1} + j$. Therefore, for each $j \in \{1, \dots, m_k\}$, $\beta_k^j \in \{1, \dots, n_{k|k-1}, n_{k|k-1} + j, \dots, n_{k|k}\}$.

To eliminate the implicit high-order factor induced by the global association hypothesis constraint, we introduce low-order consistency factors between the object-oriented α_k and the measurement-oriented β_k association variables. Specifically, for each valid pair (i, j) , we define

$$\Psi_k^{i,j}(\alpha_k^{i,j}, \beta_k^j) = \begin{cases} 1 & \alpha_k^{i,j} = 1, \beta_k^j = i \\ 1 & \alpha_k^{i,j} = 0, \beta_k^j \neq i \\ 0 & \text{otherwise.} \end{cases} \quad (38)$$

This factor enforces that the dual representations of the data association agree locally on whether the j -th measurement z_k^j is associated with the i -th Bernoulli component. Consequently, the original global hypothesis constraint in (11) is now represented explicitly through a product of consistency factors between the dual association variables, thereby transforming the remaining high-order dependency into a BP-friendly local factorization.

By plugging (32) and (33) into (21) and using the low-order consistency factors between the dual representation of data association, we can factorize the joint posterior of the set of objects $\tilde{\mathbf{x}}_k$, object detection variables $D_k^{1:n_{k|k-1}}$, object-oriented α_k and measurement-oriented β_k association variables as in (39). The factor graph corresponding to this factorized joint posterior is illustrated in Fig. 1.

$$\begin{aligned} & f_{k|k}(\tilde{\mathbf{x}}_k, D_k^{1:n_{k|k-1}}, \alpha_k, \beta_k) \\ & \propto f_{k|k}^p(\tilde{\mathbf{x}}_k^u) \prod_{i=1}^{n_{k|k-1}} \left[f_k^{D,i}(D_k^i | \tilde{\mathbf{x}}_k^i) f_{k|k-1}^i(\tilde{\mathbf{x}}_k^i) \prod_{j=1}^{m_k} \Phi_k^{i,j}(D_k^i, \alpha_k^{i,j}) \right] \prod_{i=n_{k|k-1}+1}^{n_{k|k}} \bar{f}_{k|k-1}^i(\tilde{\mathbf{x}}_k^i) \\ & \quad \times \prod_{j=1}^{m_k} \left[\bar{s}_k^{n_{k|k-1}+j}(\tilde{\mathbf{x}}_k^{n_{k|k-1}+j}, \alpha_k^{n_{k|k-1}+j,j}, z_k^j) \prod_{\substack{i \in \{1, \dots, n_{k|k-1}\} \cup \\ \{n_{k|k-1}+j+1, \dots, n_{k|k}\}}} \bar{s}_k^i(\tilde{\mathbf{x}}_k^i, \alpha_k^{i,j}, z_k^j) \prod_{\substack{i \in \{1, \dots, n_{k|k-1}\} \cup \\ \{n_{k|k-1}+j, \dots, n_{k|k}\}}} \Psi_k^{i,j}(\alpha_k^{i,j}, \beta_k^j) \right]. \end{aligned} \quad (39)$$

Remark 1. In Fig. 1, we can notice that, for each new Bernoulli component $i \in \{n_{k|k-1} + 1, \dots, n_{k|k}\}$, each object-oriented association variable node $\alpha_k^{i,j}$ is connected to two factor nodes, $\tilde{\mathbf{x}}_k^i$ and β_k^j . This suggests that each variable node $\alpha_k^{i,j}$ and its two neighboring factor nodes can be combined into a single factor node that directly connects variable nodes $\tilde{\mathbf{x}}_k^i$ and β_k^j , by marginalizing out the object-oriented association variables $\alpha_k^{i,j}$ for new Bernoulli components from the joint posterior. This observation leads to a simpler but equivalent factor graph for the new Bernoulli components. Nevertheless, for clarity, in the next section we will derive the loopy BP recursions using the factor graph in Fig. 1, which allows the message passing equations for existing and new Bernoulli components to be written in a similar form. In implementation, the relevant messages for new Bernoulli components can still be collapsed by marginalizing out $\alpha_k^{i,j}$, so the computational complexity remains unchanged.

Remark 2. Compared with the factor graph for the Poisson measurement model in [17, Fig. 2], the factor graph for the ZIP model in Fig. 1 contains additional ingredients: the detection variables D_k^i and factors $f_k^{D,i}$ for the existing Bernoulli components, the object-oriented association variables α_k , as well as the consistency factors $\Phi_k^{i,j}$ and $\Psi_k^{i,j}$. The reason is that, for the Poisson measurement model, the object-generated measurement set density factorizes directly over individual measurements, so that the posterior can be expressed solely in terms of the measurement-oriented association variables β_k . In the ZIP case, however, the object detection event needs to be modeled explicitly, which introduces an additional dependency between object detection and measurement associations. Retaining the object-oriented association variables therefore provides a convenient way to expose this structure through low-order factors.

IV. LOOPY BELIEF PROPAGATION

The objective is to compute the marginal Bernoulli density $f_{k|k}^i(\tilde{\mathbf{x}}_k^i)$, cf. (9b), for $i \in \{1, \dots, n_{k|k}\}$. Since the factor graph in Fig. 1 contains cycles, exact BP is no longer applicable, and we instead resort to loopy BP, with all messages updated in parallel

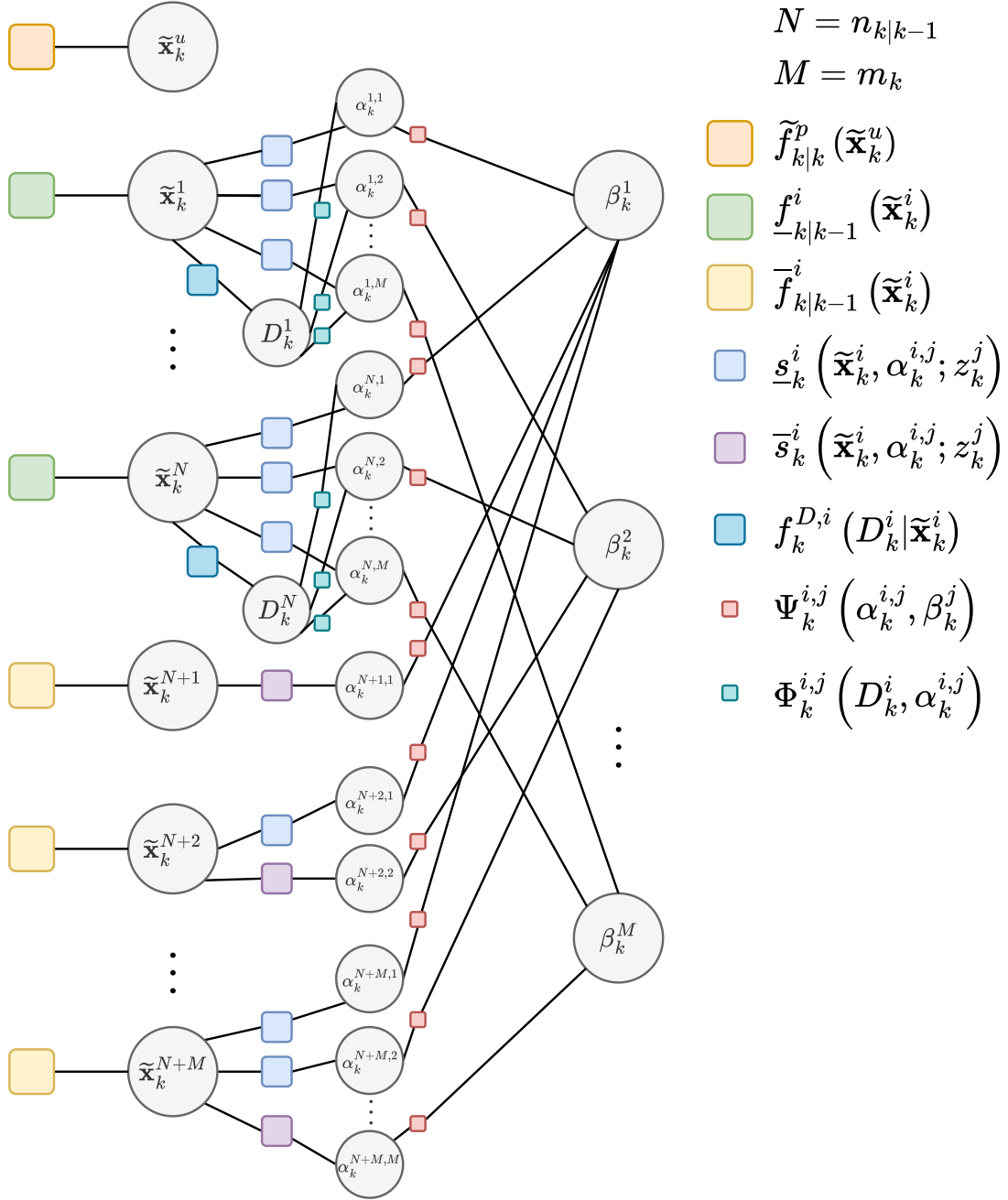


Fig. 1. Factor graph for the factorized joint posterior (39), where variable and factor nodes are represented using circles and squares, respectively.

as in [17], [19]. In this section, we present the resulting message passing and belief update equations. For notational simplicity, the time index is omitted from all messages. Also, whenever the Kronecker delta function $\delta_i[u]$ has fixed the auxiliary variable to $u = i$, we use the shorthand $\{(i, x)\}$ for the corresponding singleton state.

1) *Extrinsic messages from Bernoulli state node to local likelihood factor node:* For an existing Bernoulli component $i \in \{1, \dots, n_{k|k-1}\}$, the extrinsic message from $\tilde{\mathbf{x}}_k^i$ to the local likelihood factor $\underline{s}_k^i(\tilde{\mathbf{x}}_k^i, \alpha_k^{i,j}; z_k^j)$ for $j \in \{1, \dots, m_k\}$ is given by

$$\epsilon^{i,j}(\tilde{\mathbf{x}}_k^i) = \underline{f}_{-k|k-1}^i(\tilde{\mathbf{x}}_k^i) \zeta^i(\tilde{\mathbf{x}}_k^i) \prod_{\substack{l=1 \\ l \neq j}}^{m_k} \varrho^{i,l}(\tilde{\mathbf{x}}_k^i), \quad (40)$$

where $\zeta^i(\tilde{\mathbf{x}}_k^i)$ represents the message sent from the detection subgraph to $\tilde{\mathbf{x}}_k^i$, and $\varrho^{i,l}(\tilde{\mathbf{x}}_k^i)$ represents the message from the l -th local likelihood branch back to $\tilde{\mathbf{x}}_k^i$.

For a new Bernoulli component $i = n_{k|k-1} + j'$, with $j' \in \{1, \dots, m_k\}$, there is no detection subgraph. In this case, the extrinsic message from $\tilde{\mathbf{x}}_k^i$ to the local likelihood factor, \underline{s}_k^i or \bar{s}_k^i , associated with measurement z_k^j where $j \in \{1, \dots, j'\}$, is given by

$$\epsilon^{i,j}(\tilde{\mathbf{x}}_k^i) = \bar{f}_{k|k-1}^i(\tilde{\mathbf{x}}_k^i) \prod_{\substack{l=1 \\ l \neq j}}^{j'} \varrho^{i,l}(\tilde{\mathbf{x}}_k^i). \quad (41)$$

The messages $\epsilon^{i,j}(\tilde{\mathbf{x}}_k^i)$ provide the state-dependent extrinsic information required to evaluate the compatibility between the i -th Bernoulli component and the j -th measurement z_k^j .

2) *Messages from local likelihood factor node to object-oriented association variable node:* For an existing Bernoulli component $i \in \{1, \dots, n_{k|k-1}\}$, the message from local likelihood factor $\underline{s}_k^i(\tilde{\mathbf{x}}_k^i, \alpha_k^{i,j}; z_k^j)$ to $\alpha_k^{i,j}$ for $j \in \{1, \dots, m_k\}$ is given by

$$\vartheta^{i,j}(\alpha_k^{i,j}) = \int \underline{s}_k^i(\tilde{\mathbf{x}}_k^i, \alpha_k^{i,j}; z_k^j) \epsilon^{i,j}(\tilde{\mathbf{x}}_k^i) \delta \tilde{\mathbf{x}}_k^i. \quad (42)$$

Using (36) and normalizing $\vartheta^{i,j}(\alpha_k^{i,j})$ by $\vartheta^{i,j}(0)$, we obtain $\bar{\vartheta}^{i,j}(0) = 1$ and

$$\bar{\vartheta}^{i,j}(1) = \frac{\int \gamma_k(x) \ell_k(z_k^j | x) \epsilon^{i,j}(\{(i, x)\}) dx}{\int \epsilon^{i,j}(\tilde{\mathbf{x}}_k^i) \delta \tilde{\mathbf{x}}_k^i}, \quad (43)$$

where for a normalized message $\epsilon^{i,j}(\tilde{\mathbf{x}}_k^i)$, $\int \epsilon^{i,j}(\tilde{\mathbf{x}}_k^i) \delta \tilde{\mathbf{x}}_k^i = 1$. Since the BP messages are only defined up to a positive scale factor, the state messages $\epsilon^{i,j}(\tilde{\mathbf{x}}_k^i)$ are normalized after each update whenever convenient.

For a new Bernoulli component $i = n_{k|k-1} + j'$, with $j' \in \{1, \dots, m_k\}$, two cases arise. If $j < j'$, the corresponding local likelihood factor is $\underline{s}_k^i(\tilde{\mathbf{x}}_k^i, \alpha_k^{i,j}; z_k^j)$, and the message is also represented by (42). If $j = j'$, the local likelihood factor is $\bar{s}_k^i(\tilde{\mathbf{x}}_k^i, \alpha_k^{i,j}; z_k^j)$, and we have

$$\vartheta^{i,j}(\alpha_k^{i,j}) = \int \bar{s}_k^i(\tilde{\mathbf{x}}_k^i, \alpha_k^{i,j}; z_k^j) \epsilon^{i,j}(\tilde{\mathbf{x}}_k^i) \delta \tilde{\mathbf{x}}_k^i. \quad (44)$$

Using (37) and normalizing $\vartheta^{i,j}(\alpha_k^{i,j})$ by $\vartheta^{i,j}(0)$, we obtain $\bar{\vartheta}^{i,j}(0) = 1$ and

$$\bar{\vartheta}^{i,j}(1) = \frac{\int \gamma_k(x) \ell_k(z_k^j | x) \epsilon^{i,j}(\{(i, x)\}) dx}{\epsilon^{i,j}(\emptyset)} + \lambda_k^C(z_k^j). \quad (45)$$

The normalized message $\bar{\vartheta}^{i,j}(\alpha_k^{i,j})$ provides a scalar measure of how compatible the i -th Bernoulli component is with measurement z_k^j , relative to the inactive case $\alpha_k^{i,j} = 0$.

3) *Messages in the object detection subgraph:* For an existing Bernoulli component $i \in \{1, \dots, n_{k|k-1}\}$, its detection subgraph has the structure

$$\tilde{\mathbf{x}}_k^i - f_k^{D,i} - D_k^i - \{\Phi_k^{i,j}\}_{j=1}^{m_k} - \{\alpha_k^{i,j}\}_{j=1}^{m_k}. \quad (46)$$

This subgraph produces two types of messages: one towards the Bernoulli state nodes $\tilde{\mathbf{x}}_k^i$, and the other towards the object-oriented association variable nodes $\alpha_k^{i,j}$.

For $i \in \{1, \dots, n_{k|k-1}\}$, $j \in \{1, \dots, m_k\}$, we let $\eta_{\Phi}^{i,j}(\alpha_k^{i,j})$ denote the incoming extrinsic message from $\alpha_k^{i,j}$ to the factor $\Phi_k^{i,j}(D_k^i, \alpha_k^{i,j})$, which is given by

$$\eta_{\Phi}^{i,j}(\alpha_k^{i,j}) = \bar{\vartheta}^{i,j}(\alpha_k^{i,j}) \xi^{i,j}(\alpha_k^{i,j}) = \begin{cases} \bar{\vartheta}^{i,j}(1) \xi^{i,j}(1) & \alpha_k^{i,j} = 1 \\ \xi^{i,j}(0) & \alpha_k^{i,j} = 0, \end{cases} \quad (47)$$

where $\xi^{i,j}$ is the message from $\Psi_k^{i,j}$ to $\alpha_k^{i,j}$, defined later in (61). Then, the message from $\Phi_k^{i,j}$ to D_k^i is

$$\mu^{i,j}(D_k^i) = \sum_{\alpha_k^{i,j} \in \{0,1\}} \Phi_k^{i,j}(D_k^i, \alpha_k^{i,j}) \eta_{\Phi}^{i,j}(\alpha_k^{i,j}) = \begin{cases} \xi^{i,j}(0) + \bar{\vartheta}^{i,j}(1) \xi^{i,j}(1) & D_k^i = 1 \\ \xi^{i,j}(0) & D_k^i = 0. \end{cases} \quad (48)$$

By combining the messages $\mu^{i,j}(D_k^i)$ over all j , the message from the detection subgraph to $\tilde{\mathbf{x}}_k^i$ is given by

$$\zeta^i(\tilde{\mathbf{x}}_k^i) = \sum_{D_k^i \in \{0,1\}} f_k^{D,i}(D_k^i | \tilde{\mathbf{x}}_k^i) \prod_{j=1}^{m_k} \mu^{i,j}(D_k^i). \quad (49)$$

Plugging (27) and (48) into (49) yields

$$\zeta^i(\tilde{\mathbf{x}}_k^i) = \begin{cases} \delta_i[u] \left[(1 - p_k^D(x)) \prod_{j=1}^{m_k} \mu^{i,j}(0) + p_k^D(x) e^{-\gamma_k(x)} \prod_{j=1}^{m_k} \mu^{i,j}(1) \right] & \tilde{\mathbf{x}}_k^i = \{(u, x)\} \\ \prod_{j=1}^{m_k} \mu^{i,j}(0) & \tilde{\mathbf{x}}_k^i = \emptyset \\ 0 & \text{otherwise.} \end{cases} \quad (50)$$

Hence, $\zeta^i(\tilde{\mathbf{x}}_k^i)$ summarizes all information flowing from the object detection variable D_k^i and the consistency factors $\Phi_k^{i,j}$ back to the Bernoulli state node $\tilde{\mathbf{x}}_k^i$.

To compute the messages from the detection subgraph to $\alpha_k^{i,j}$, we first form the extrinsic messages from D_k^i to $\Phi_k^{i,j}$,

$$\nu^{i,j}(D_k^i) = \prod_{\substack{l=1 \\ l \neq j}}^{m_k} \mu^{i,l}(D_k^i) \int f_k^{D,i}(D_k^i | \tilde{\mathbf{x}}_k^i) \chi^i(\tilde{\mathbf{x}}_k^i) \delta \tilde{\mathbf{x}}_k^i, \quad (51)$$

where χ^i is the message from $\tilde{\mathbf{x}}_k^i$ to $f_k^{D,i}$, given by

$$\chi^i(\tilde{\mathbf{x}}_k^i) = f_{-k|k-1}^i(\tilde{\mathbf{x}}_k^i) \prod_{j=1}^{m_k} \varrho^{i,j}(\tilde{\mathbf{x}}_k^i). \quad (52)$$

Using the definition of $f_k^{D,i}$ (27), we obtain

$$\nu^{i,j}(1) = \prod_{\substack{l=1 \\ l \neq j}}^{m_k} \mu^{i,l}(1) \int p_k^D(x) e^{-\gamma_k(x)} \chi^i(\{(i, x)\}) dx, \quad (53)$$

$$\nu^{i,j}(0) = \prod_{\substack{l=1 \\ l \neq j}}^{m_k} \mu^{i,l}(0) \left[\int (1 - p_k^D(x)) \chi^i(\{(i, x)\}) dx + \chi^i(\emptyset) \right]. \quad (54)$$

Finally, the message from $\Phi_k^{i,j}$ to $\alpha_k^{i,j}$ is

$$\lambda^{i,j}(\alpha_k^{i,j}) = \sum_{D_k^i \in \{0,1\}} \Phi_k^{i,j}(D_k^i, \alpha_k^{i,j}) \nu^{i,j}(D_k^i). \quad (55)$$

Using (31) and normalizing $\lambda^{i,j}(\alpha_k^{i,j})$ by $\lambda^{i,j}(0)$, we obtain $\bar{\lambda}^{i,j}(0) = 1$ and

$$\bar{\lambda}^{i,j}(1) = \frac{\nu^{i,j}(1)}{\nu^{i,j}(0) + \nu^{i,j}(1)}. \quad (56)$$

Here, the normalized message $\bar{\lambda}^{i,j}(\alpha_k^{i,j})$ quantifies, for the i -th existing Bernoulli component, the compatibility between the detection event D_k^i and the assignment of measurement z_k^j to that component.

4) *Messages through the association consistency factor:* For each measurement z_k^j , $j \in \{1, \dots, m_k\}$, we denote the admissible support of β_k^j as $\mathcal{I}_j = \{1, \dots, n_{k|k-1}, n_{k|k-1} + j, \dots, n_{k|k}\}$. The incoming extrinsic message from $\alpha_k^{i,j}$ to $\Psi_k^{i,j}$ is obtained by combining the messages passed from the local likelihood factor and the object detection consistency factor. Specifically, for an existing Bernoulli component $i \in \{1, \dots, n_{k|k-1}\}$, with $j \in \{1, \dots, m_k\}$,

$$\eta_{\Psi}^{i,j}(\alpha_k^{i,j}) = \bar{\vartheta}^{i,j}(\alpha_k^{i,j}) \bar{\lambda}^{i,j}(\alpha_k^{i,j}). \quad (57)$$

For a new Bernoulli component $i = n_{k|k-1} + j'$, with $j' \in \{1, \dots, m_k\}$, $j \in \{1, \dots, j'\}$,

$$\eta_{\Psi}^{i,j}(\alpha_k^{i,j}) = \bar{\vartheta}^{i,j}(\alpha_k^{i,j}). \quad (58)$$

The message from $\Psi_k^{i,j}$ to β_k^j is

$$\kappa^{i,j}(\beta_k^j) = \sum_{\alpha_k^{i,j} \in \{0,1\}} \Psi_k^{i,j}(\alpha_k^{i,j}, \beta_k^j) \eta_{\Psi}^{i,j}(\alpha_k^{i,j}) = \begin{cases} \eta_{\Psi}^{i,j}(1) & \beta_k^j = i \\ 1 & \beta_k^j \neq i. \end{cases} \quad (59)$$

The message from β_k^j back to $\Psi_k^{i,j}$ is given by the product of all incoming messages to β_k^j , excluding the one from $\Psi_k^{i,j}$,

$$\rho^{i,j}(\beta_k^j) = \prod_{l \in \mathcal{I}_j \setminus \{i\}} \kappa^{l,j}(\beta_k^j) = \begin{cases} 1 & \beta_k^j = i \\ \eta_{\Psi}^{\beta_k^j,j}(1) & \beta_k^j \in \mathcal{I}_j \setminus \{i\}. \end{cases} \quad (60)$$

The message from $\Psi_k^{i,j}$ to $\alpha_k^{i,j}$ is then

$$\xi^{i,j}(\alpha_k^{i,j}) = \sum_{\beta_k^j \in \mathcal{I}_j} \Psi_k^{i,j}(\alpha_k^{i,j}, \beta_k^j) \rho^{i,j}(\beta_k^j) = \begin{cases} 1 & \alpha_k^{i,j} = 1 \\ \sum_{l \in \mathcal{I}_j \setminus \{i\}} \eta_{\Psi}^{l,j}(1) & \alpha_k^{i,j} = 0. \end{cases} \quad (61)$$

Here, the messages $\kappa^{i,j}(\beta_k^j)$ and $\xi^{i,j}(\alpha_k^{i,j})$ quantify the local agreement enforced by the consistency factor $\Psi_k^{i,j}$ between the dual data association representations.

5) *Messages from local likelihood factor node to Bernoulli state node:* To compute the message $\varrho^{i,j}(\tilde{\mathbf{x}}_k^i)$ from the j -th local likelihood branch back to $\tilde{\mathbf{x}}_k^i$, we first combine the incoming messages at $\alpha_k^{i,j}$. Specifically, for existing Bernoulli component $i \in \{1, \dots, n_{k|k-1}\}$, with $j \in \{1, \dots, m_k\}$,

$$\tau^{i,j}(\alpha_k^{i,j}) = \bar{\lambda}^{i,j}(\alpha_k^{i,j}) \xi^{i,j}(\alpha_k^{i,j}). \quad (62)$$

For a new Bernoulli component $i = n_{k|k-1} + j'$, with $j' \in \{1, \dots, m_k\}$, $j \in \{1, \dots, j'\}$,

$$\tau^{i,j}(\alpha_k^{i,j}) = \xi^{i,j}(\alpha_k^{i,j}). \quad (63)$$

Then, for factors of type $\underline{s}_k^i(\tilde{\mathbf{x}}_k^i, \alpha_k^{i,j}; z_k^j)$, we have

$$\varrho^{i,j}(\tilde{\mathbf{x}}_k^i) = \sum_{\alpha_k^{i,j} \in \{0,1\}} \underline{s}_k^i(\tilde{\mathbf{x}}_k^i, \alpha_k^{i,j}; z_k^j) \tau^{i,j}(\alpha_k^{i,j}) = \begin{cases} \delta_i[u] \gamma_k(x) \ell_k(z_k^j|x) \tau^{i,j}(1) + \tau^{i,j}(0), & \tilde{\mathbf{x}}_k^i = \{(u, x)\} \\ \tau^{i,j}(0) & \tilde{\mathbf{x}}_k^i = \emptyset \\ 0 & \text{otherwise.} \end{cases} \quad (64)$$

For factor $\bar{s}_k^i(\tilde{\mathbf{x}}_k^i, \alpha_k^{i,j}; z_k^j)$ of a new Bernoulli component $i = n_{k|k-1} + j$, we similarly obtain

$$\varrho^{i,j}(\tilde{\mathbf{x}}_k^i) = \sum_{\alpha_k^{i,j} \in \{0,1\}} \bar{s}_k^i(\tilde{\mathbf{x}}_k^i, \alpha_k^{i,j}; z_k^j) \tau^{i,j}(\alpha_k^{i,j}) = \begin{cases} \delta_i[u] \gamma_k(x) \ell_k(z_k^j|x) \tau^{i,j}(1) & \tilde{\mathbf{x}}_k^i = \{(u, x)\} \\ \lambda_k^C(z_k^j) \tau^{i,j}(1) + \tau^{i,j}(0) & \tilde{\mathbf{x}}_k^i = \emptyset \\ 0, & \text{otherwise.} \end{cases} \quad (65)$$

Therefore, the message $\varrho^{i,j}(\tilde{\mathbf{x}}_k^i)$ summarizes the contribution of the j -th local likelihood branch to the Bernoulli state variable $\tilde{\mathbf{x}}_k^i$, after combining the local measurement compatibility with the association-side consistency information.

6) *Belief calculations:* The belief of each Bernoulli state variable $\tilde{\mathbf{x}}_k^i$ is obtained by multiplying all incoming messages, together with the corresponding prior factor. For an existing Bernoulli component $i \in \{1, \dots, n_{k|k-1}\}$, the belief is

$$b^i(\tilde{\mathbf{x}}_k^i) \propto \underline{f}_{k|k-1}^i(\tilde{\mathbf{x}}_k^i) \zeta^i(\tilde{\mathbf{x}}_k^i) \prod_{j=1}^{m_k} \varrho^{i,j}(\tilde{\mathbf{x}}_k^i), \quad (66)$$

where $\zeta^i(\tilde{\mathbf{x}}_k^i)$ (50) is the collapsed message from the detection subgraph. For a new Bernoulli component $i = n_{k|k-1} + j'$, with $j' \in \{1, \dots, m_k\}$, the belief is

$$b^i(\tilde{\mathbf{x}}_k^i) \propto \bar{f}_{k|k-1}^i(\tilde{\mathbf{x}}_k^i) \prod_{j=1}^{j'} \varrho^{i,j}(\tilde{\mathbf{x}}_k^i). \quad (67)$$

After normalization, the beliefs in (66) and (67) provide the loopy BP approximation of the marginal Bernoulli densities $f_{k|k}^i(\tilde{\mathbf{x}}_k^i)$, $i \in \{1, \dots, n_{k|k}\}$. In particular, the approximate existence probability and conditional single object density of the i -th Bernoulli component can be recovered directly from the corresponding belief $b^i(\tilde{\mathbf{x}}_k^i)$.

7) *Initialization:* To initialize loopy BP, we can first compute the extrinsic messages (40) and (41) from Bernoulli state variables $\tilde{\mathbf{x}}_k^i$ to local likelihood factors, \underline{s}_k^i or \bar{s}_k^i , according to the case of misdetection. Specifically, for an existing Bernoulli component $i \in \{1, \dots, n_{k|k-1}\}$, such initialization is induced by the prior factor (34), together with the no-association branch in the ZIP model (27), for all $j \in \{1, \dots, m_k\}$, which is given by

$$\epsilon^{i,j}(\tilde{\mathbf{x}}_k^i) = \underline{f}_{k|k-1}^i(\tilde{\mathbf{x}}_k^i) \sum_{D_k^i \in \{0,1\}} f_k^{D,i}(D_k^i|\tilde{\mathbf{x}}_k^i). \quad (68)$$

As for new Bernoulli components, the initialization is induced by the prior factor (35). In addition, the message χ^i from the Bernoulli state variable $\tilde{\mathbf{x}}_k^i$ to the factor $f_k^{D,i}$ is initialized as $\chi^i(\tilde{\mathbf{x}}_k^i) = \underline{f}_{k|k-1}^i(\tilde{\mathbf{x}}_k^i)$, cf. (52).

With these initialized messages in place, the remaining messages are computed from the corresponding recursions, and all the messages are then updated in parallel. The iterations are repeated either for a fixed number of iterations or until convergence. After termination, the beliefs $b^i(\tilde{\mathbf{x}}_k^i)$, $i \in \{1, \dots, n_{k|k}\}$, provide the approximate marginal Bernoulli densities.

V. PARTICLE IMPLEMENTATION

In this section, we present a particle-based loopy BP implementation of the extended object PMB filter under the ZIP measurement model, where each Bernoulli component is represented by an existence probability and a particle representation of its single object density. We first describe the prediction step, and then present the implementation of the loopy BP update derived in Section IV. We also discuss several practical aspects of the implementation.

We represent the PMB density at time step $k' \in \{k-1, k\}$ using a hybrid form. The PPP intensity for undetected objects is kept in analytic form as $\lambda_{k|k'}(x)$, whereas each Bernoulli component is represented by its existence probability $r_{k|k'}^i$ and a particle approximation of its single object density,

$$f_{k|k'}^i(x) = \sum_{l=1}^L w_{k|k'}^{i,(l)} \delta_{x_{k|k'}^{i,(l)}}(x), \quad (69)$$

where L is the number of particles, $x_{k|k'}^{i,(l)}$ is the l -th particle, $w_{k|k'}^{i,(l)}$ is its normalized weight such that $\sum_{l=1}^L w_{k|k'}^{i,(l)} = 1$. In what follows, we omit the auxiliary variable u in the object state for simplicity.

A. Prediction Step

The PPP intensity for undetected objects is predicted analytically according to (12a) in Lemma 1. In contrast, the Bernoulli components are propagated over time by particles. Specifically, let the i -th Bernoulli component, with $i \in \{1, \dots, n_{k-1|k-1}\}$, at time step $k-1$ be represented by

$$\left\{ r_{k-1|k-1}^i, \left(w_{k-1|k-1}^{i,(l)}, x_{k-1|k-1}^{i,(l)} \right)_{l=1}^L \right\}. \quad (70)$$

For each particle $x_{k-1|k-1}^{i,(l)}$, to compute its predicted state at time step k , we draw a predicted particle $x_{k|k-1}^{i,(l)}$ from a proposal density $q_{k|k-1}^i(\cdot | x_{k-1|k-1}^{i,(l)})$, and its corresponding unnormalized importance weight is given by

$$\tilde{w}_{k|k-1}^{i,(l)} = w_{k-1|k-1}^{i,(l)} \frac{p_k^S(x_{k-1|k-1}^{i,(l)}) g_k(x_{k|k-1}^{i,(l)} | x_{k-1|k-1}^{i,(l)})}{q_{k|k-1}^i(x_{k|k-1}^{i,(l)} | x_{k-1|k-1}^{i,(l)})}, \quad (71)$$

and is normalized as

$$w_{k|k-1}^{i,(l)} = \frac{\tilde{w}_{k|k-1}^{i,(l)}}{\sum_{l'=1}^L \tilde{w}_{k|k-1}^{i,(l')}}. \quad (72)$$

The predicted existence probability is given by

$$r_{k|k-1}^i = r_{k-1|k-1}^i \sum_{l=1}^L w_{k-1|k-1}^{i,(l)} p_k^S(x_{k-1|k-1}^{i,(l)}). \quad (73)$$

The i -th predicted Bernoulli density, with $i \in \{1, \dots, n_{k|k-1}\}$, is then represented by

$$\left\{ r_{k|k-1}^i, \left(w_{k|k-1}^{i,(l)}, x_{k|k-1}^{i,(l)} \right)_{l=1}^L \right\}, \quad (74)$$

where $n_{k|k-1} = n_{k-1|k-1}$.

B. Update Step

We now describe the particle implementation of the update step that includes initialization, sum-product message passing, and belief calculation. We note that in each iteration of loopy BP, the particle states remain unchanged, but their weights are refined. For the (normalized) extrinsic message $\epsilon^{i,j,(p)}(\tilde{\mathbf{x}}_k^i)$ at the p -th iteration, it is parameterized by

$$\left\{ r_{k,\epsilon}^{i,j,(p)}, \left(w_{k,\epsilon}^{i,j,(l),(p)}, x_{k|k}^{i,(l)} \right)_{l=1}^L \right\}, \quad (75)$$

and the (normalized) message $\chi^i(\tilde{\mathbf{x}}_k^i)$ at the p -th iteration is parameterized by

$$\left\{ r_{k,\chi}^{i,(p)}, \left(w_{k,\chi}^{i,(l),(p)}, x_{k|k}^{i,(l)} \right)_{l=1}^L \right\}. \quad (76)$$

1) *Initialization*: For the i -th existing Bernoulli component, its extrinsic messages $\epsilon^{i,j,(1)}(\tilde{\mathbf{x}}_k^i)$, $j \in \{1, \dots, m_k\}$ at the first iteration are initialized according to (68). Specifically, we have $x_{k|k}^{i,(l)} = x_{k|k-1}^{i,(l)}$ for $l \in \{1, \dots, L\}$, and for each particle $x_{k|k}^{i,(l)}$, its unnormalized weight is

$$\tilde{w}_{k,\epsilon}^{i,j,(l),(1)} = w_{k|k-1}^{i,(l)} \left[1 - p_k^D \left(x_{k|k}^{i,(l)} \right) + p_k^D \left(x_{k|k}^{i,(l)} \right) e^{-\gamma_k \left(x_{k|k}^{i,(l)} \right)} \right], \quad (77)$$

which are identical for all $j \in \{1, \dots, m_k\}$ and normalized as

$$w_{k,\epsilon}^{i,j,(l),(1)} = \frac{\tilde{w}_{k,\epsilon}^{i,j,(l),(1)}}{\sum_{l'=1}^L \tilde{w}_{k,\epsilon}^{i,j,(l'),(1)}}. \quad (78)$$

The initial existence probability of the i -th existing Bernoulli component is given by

$$r_{k,\epsilon}^{i,j,(1)} = \frac{r_{k|k-1}^i \sum_{l=1}^L \tilde{w}_{k,\epsilon}^{i,j,(l),(1)}}{1 - r_{k|k-1}^i + r_{k|k-1}^i \sum_{l=1}^L \tilde{w}_{k,\epsilon}^{i,j,(l),(1)}}. \quad (79)$$

In addition, the message $\chi^i(\tilde{\mathbf{x}}_k^i)$ (76) is initialized as (74).

As for a new Bernoulli component $i = n_{k|k-1} + j'$, with $j' \in \{1, \dots, m_k\}$, to initialize its extrinsic messages $\epsilon^{i,j,(1)}(\tilde{\mathbf{x}}_k^i)$ for $j \in \{1, \dots, j'\}$, we first draw the particles $\{x_{k|k}^{i,(l)}\}_{l=1}^L$ from a proposal density $\bar{q}_k^i(x)$. According to (35), the corresponding unnormalized importance weights are

$$\tilde{w}_{k,\epsilon}^{i,j,(l),(1)} = \frac{p_k^D \left(x_{k|k}^{i,(l)} \right) e^{-\gamma_k \left(x_{k|k}^{i,(l)} \right)} \lambda_{k|k-1} \left(x_{k|k}^{i,(l)} \right)}{\bar{q}_k^i \left(x_{k|k}^{i,(l)} \right)}, \quad (80)$$

which are identical for all valid j and normalized as in (78), and the initial existence probability of the i -th new Bernoulli component is given by

$$r_{k,\epsilon}^{i,j,(1)} = \frac{\sum_{l=1}^L \tilde{w}_{k,\epsilon}^{i,j,(l),(1)}}{1 + \sum_{l=1}^L \tilde{w}_{k,\epsilon}^{i,j,(l),(1)}}. \quad (81)$$

2) *Sum-product message passing*: For an existing Bernoulli component $i \in \{1, \dots, n_{k|k-1}\}$, the message from \underline{s}_k^i to $\alpha_k^{i,j}$ (43) for $j \in \{1, \dots, m_k\}$ is given by

$$\bar{\vartheta}^{i,j,(p)}(1) \approx r_{k,\epsilon}^{i,j,(p)} \sum_{l=1}^L w_{k,\epsilon}^{i,j,(l),(p)} \gamma_k \left(x_{k|k}^{i,(l)} \right) \ell_k \left(z_k^j | x_{k|k}^{i,(l)} \right). \quad (82)$$

For a new Bernoulli component $i = n_{k|k-1} + j'$, with $j' \in \{1, \dots, m_k\}$ and $j < j'$, the message from \underline{s}_k^i to $\alpha_k^{i,j}$ (43) is also given by (82). The message from \bar{s}_k^i to $\alpha_k^{i,j}$ (45) when $j = j'$ is given by

$$\bar{\vartheta}^{i,j,(p)}(1) \approx \frac{r_{k,\epsilon}^{i,j,(p)} \sum_{l=1}^L w_{k,\epsilon}^{i,j,(l),(p)} \gamma_k \left(x_{k|k}^{i,(l)} \right) \ell_k \left(z_k^j | x_{k|k}^{i,(l)} \right)}{1 - r_{k,\epsilon}^{i,j,(p)}} + \lambda_k^C \left(z_k^j \right). \quad (83)$$

For an existing Bernoulli component, the message from D_k^i to $\Phi_k^{i,j}$ (53) is given by

$$\nu^{i,j,(p)}(1) = \prod_{\substack{j'=1 \\ j' \neq j}}^{m_k} \mu^{i,j',(p)}(1) \left[r_{k,\chi}^{i,(p)} \sum_{l=1}^L w_{k,\chi}^{i,(l),(p)} p_k^D \left(x_{k|k}^{i,(l)} \right) e^{-\gamma_k \left(x_{k|k}^{i,(l)} \right)} \right], \quad (84)$$

$$\nu^{i,j,(p)}(0) = \prod_{\substack{j'=1 \\ j' \neq j}}^{m_k} \mu^{i,j',(p)}(0) \left[1 - r_{k,\chi}^{i,(p)} \sum_{l=1}^L w_{k,\chi}^{i,(l),(p)} p_k^D \left(x_{k|k}^{i,(l)} \right) \right]. \quad (85)$$

The remaining messages $\mu^{i,j}$, $\lambda^{i,j}$, $\kappa^{i,j}$, $\rho^{i,j}$, $\xi^{i,j}$, and $\tau^{i,j}$ are all scalar and are updated exactly according to the recursions in Section IV. Also, according to (50), the message $\zeta^i(\tilde{\mathbf{x}}_k^i)$ can be evaluated on each particle $x_{k|k}^{i,(l)}$ using the scalar message $\mu^{i,j}$. Similarly, using (64) or (65), the message $\varrho^{i,j}(\tilde{\mathbf{x}}_k^i)$ can be evaluated on each particle $x_{k|k}^{i,(l)}$ using the scalar message $\tau^{i,j}$. Consequently, the updated extrinsic messages $\epsilon^{i,j,(p+1)}(\tilde{\mathbf{x}}_k^i)$ at the next iteration are represented on the same particle support

by updated particle weights for $i \in \{1, \dots, n_{k|k}\}$ using (40) or (41). Specifically, for the case of (40) with index pair (i, j) , with $i \in \{1, \dots, n_{k|k-1}\}$, $j \in \{1, \dots, m_k\}$, the unnormalized weight of particle $x^{i,(l)}$ is

$$\tilde{w}_{k,\epsilon}^{i,j,(l),(p+1)} = w_{k|k-1}^{i,(l)} \zeta^{i,(p)} \left(\{(i, x_{k|k}^{i,(l)})\} \right) \prod_{\substack{l'=1 \\ l' \neq j}}^{m_k} \varrho^{i,l',(p)} \left(\{(i, x_{k|k}^{i,(l)})\} \right), \quad (86)$$

which is normalized as

$$w_{k,\epsilon}^{i,j,(l),(p+1)} = \frac{\tilde{w}_{k,\epsilon}^{i,j,(l),(p+1)}}{\sum_{l'=1}^L \tilde{w}_{k,\epsilon}^{i,j,(l'),(p+1)}}. \quad (87)$$

When $\epsilon^{i,j,(p+1)}(\tilde{\mathbf{x}}_k^i)$ is evaluated at an empty set, we have

$$\tilde{w}_{\emptyset}^{i,j,(p+1)} = \left(1 - r_{k|k-1}^i\right) \zeta^{i,(p)}(\emptyset) \prod_{\substack{l'=1 \\ l' \neq j}}^{m_k} \varrho^{i,l',(p)}(\emptyset). \quad (88)$$

After normalization, the existence probability of the extrinsic message $\epsilon^{i,j,(p+1)}(\tilde{\mathbf{x}}_k^i)$ (40) is given by

$$r_{k,\epsilon}^{i,j,(p+1)} = \frac{r_{k|k-1}^i \sum_{l=1}^L \tilde{w}_{k,\epsilon}^{i,j,(l),(p+1)}}{r_{k|k-1}^i \sum_{l=1}^L \tilde{w}_{k,\epsilon}^{i,j,(l),(p+1)} + \tilde{w}_{\emptyset}^{i,j,(p+1)}}. \quad (89)$$

For the case of (41) with index pair (i, j) , $i = n_{k|k-1} + j'$, $j' \in \{1, \dots, m_k\}$, and $j \in \{1, \dots, j'\}$, the unnormalized weight of particle $x_{k|k}^{i,(l)}$ is

$$\tilde{w}_{k,\epsilon}^{i,j,(l),(p+1)} = w_{k,\epsilon}^{i,j,(l),(1)} \prod_{\substack{l'=1 \\ l' \neq j}}^{j'} \varrho^{i,l',(p)} \left(\{(i, x_{k|k}^{i,(l)})\} \right), \quad (90)$$

with $w_{k,\epsilon}^{i,j,(l),(1)}$ given in (78), and its normalized weight is also computed as in (87). Similarly, when evaluated at an empty set, we have

$$\tilde{w}_{\emptyset}^{i,j,(p+1)} = \left(1 - r_{k,\epsilon}^{i,j,(1)}\right) \prod_{\substack{l'=1 \\ l' \neq j}}^{j'} \varrho^{i,l',(p)}(\emptyset), \quad (91)$$

with $r_{k,\epsilon}^{i,j,(1)}$ specified in (81), and the existence probability of the extrinsic message $\epsilon^{i,j,(p+1)}(\tilde{\mathbf{x}}_k^i)$ (41) after normalization is also computed as in (89), but with $r_{k|k-1}^i$ replaced by $r_{k,\epsilon}^{i,j,(1)}$.

In addition, for the i -th existing Bernoulli component with $i \in \{1, \dots, n_{k|k-1}\}$, the message $\chi^i(\tilde{\mathbf{x}}_k^i)$ in the detection subgraph from $\tilde{\mathbf{x}}_k^i$ to $f_k^{D,i}$ at the next iteration is also represented using the same particle support by updated particle weights. According to (52), the unnormalized weight of particle $x^{i,(l)}$ is

$$\tilde{w}_{k,\chi}^{i,(l),(p+1)} = w_{k|k-1}^{i,(l)} \prod_{j=1}^{m_k} \varrho^{i,j,(p)} \left(\{(i, x_{k|k}^{i,(l)})\} \right), \quad (92)$$

which is normalized as

$$w_{k,\chi}^{i,(l),(p+1)} = \frac{\tilde{w}_{k,\chi}^{i,(l),(p+1)}}{\sum_{l'=1}^L \tilde{w}_{k,\chi}^{i,(l'),(p+1)}}. \quad (93)$$

When $\chi^{i,(p+1)}(\tilde{\mathbf{x}}_k^i)$ is evaluated at an empty set, we have

$$\tilde{w}_{\emptyset}^{i,(p+1)} = \left(1 - r_{k|k-1}^i\right) \prod_{j=1}^{m_k} \varrho^{i,j,(p)}(\emptyset). \quad (94)$$

After normalization, the existence probability of the message $\chi^{i,(p+1)}(\tilde{\mathbf{x}}_k^i)$ (52) is given by

$$r_{k,\chi}^{i,(p+1)} = \frac{r_{k|k-1}^i \sum_{l=1}^L \tilde{w}_{k,\chi}^{i,(l),(p+1)}}{r_{k|k-1}^i \sum_{l=1}^L \tilde{w}_{k,\chi}^{i,(l),(p+1)} + \tilde{w}_{\emptyset}^{i,(p+1)}}. \quad (95)$$

3) *Belief calculation:* At the last iteration, we compute the beliefs $b^i(\tilde{\mathbf{x}}_k^i)$ for $i \in \{1, \dots, n_{k|k}\}$. Each belief is a Bernoulli set density, which can be calculated similarly to the extrinsic messages $\epsilon^{i,j,(p+1)}(\tilde{\mathbf{x}}_k^i)$ with the difference that the products in (86), (88), (90) and (91) now need to enumerate every element.

C. Practical Considerations

First, we comment on the convergence of loopy BP. Since the factor graph in Fig. 1 contains cycles, there is in general no theoretical guarantee that the parallel message passing recursions converge. Nevertheless, empirical results have shown that the proposed loopy BP update typically provides reasonable performance after only a few iterations.

Next, we briefly discuss the computational complexities. Given a fixed number of particles, the message passing complexity scales only linearly with the number of Bernoulli components and the number of measurements, as in the case of Poisson measurements [19]. However, since each measurement creates a new Bernoulli component, and an extended object typically generates multiple measurements, the overall computational complexity can conservatively be regarded as quadratic in the numbers of objects and measurements [26]. For computational tractability, Bernoulli components with existence probability smaller than a threshold are pruned, and the complexity can be reduced further by censoring messages and reordering the measurements, see [26] for details.

For particle-based implementations, the quality of the proposal density is important. Specifically, for new Bernoulli components, instead of drawing particles from a non-informative proposal, e.g., a uniform density for the locations, one may use a measurement-driven proposal density that depends on the associated measurement or measurement cluster. This is especially useful for state components that are directly informed by the measurements. In addition, systematic resampling is applied when needed in order to alleviate particle degeneracy [27].

Lastly, for state estimation, we extract object estimates from Bernoulli components whose existence probabilities exceed a threshold. For each such Bernoulli component, the estimate is obtained from the weighted particle set, e.g., by weighted averaging of the state components.

VI. SIMULATIONS AND RESULTS

In this section, we present the results from a Monte Carlo simulation study with 100 runs where the performance of the following four multiple extended object filters are compared²:

- The proposed extended object PMB filter under the ZIP measurement model, referred to as PMB-BP-ZIP.
- The extended object PMB filter under the Poisson measurement model with BP, referred to as PMB-BP-PPP.
- The extended object PMBM filter under the ZIP measurement model with sampling-based data association [18], referred to as PMBM-SO-ZIP.
- The extended object PMB filter under the ZIP measurement model with sampling-based data association [18], referred to as PMB-SO-ZIP.

We consider the random matrix model for EOT, where the object has an elliptical shape modeled by a symmetric positive definite matrix [28]. The random matrix model has been used in several PMBM and PMB implementations [11], [12], [17], [18], thereby making the comparison easy.

The single object state is $x_k = (e_k, E_k, \gamma_k)$, consisting of the kinematic state $e_k \in \mathbb{R}^4$, a 2×2 symmetric positive definite matrix representing the extent state E_k , and the Poisson object measurement rate $\gamma_k > 0$. The kinematic state e_k consists of 2D position and velocity. We assume that each object moves according to a nearly constant velocity motion model, and that its extent and measurement rate remain unchanged over time. The kinematic state transition density is

$$g_k(e_k|e_{k-1}) = \mathcal{N}(e_k; Fe_{k-1}, Q), \quad F = I_2 \otimes \begin{bmatrix} 1 & T \\ 0 & 1 \end{bmatrix}, \quad Q = \sigma_q^2 I_2 \otimes \begin{bmatrix} T^3/3 & T^2/2 \\ T^2/2 & T \end{bmatrix},$$

where I_2 is the 2×2 identity matrix, $T = 0.2$ is the sampling interval, and $\sigma_q = 0.8$ is the process noise standard deviation.

We consider the same scenario as in [17], [19] with a region of interest of size $[-150 \text{ m}, 150 \text{ m}] \times [-150 \text{ m}, 150 \text{ m}]$, where ten objects start moving towards the center from positions uniformly placed on a circle of radius 125 m around the center with an initial velocity 12.5 m/s, and then they become closely-spaced for some time before they separate. The initial extent matrix of each object is obtained by sampling from an inverse-Wishart distribution with degree of freedom 100 and mean matrix $5I_2$. The true object trajectories are illustrated in Fig. 1. The object survival probability is $p^S = 0.99$.

PMB-BP-ZIP and PMB-BP-PPP use particle implementations, whereas PMBM-SO-ZIP and PMB-SO-ZIP adopt analytical GGIW implementations [11]. For all the implementations, the Poisson birth rate is 0.01. In the birth density, the velocity is Gaussian distributed with zero mean and covariance $225I_2$, the extent is inverse-Wishart distributed with mean $5I_2$ and degree of freedom 100, and the Poisson object measurement rate is Gamma distributed with mean γ and rate parameter 100. For the position, it is Gaussian distributed with zero mean and covariance $150^2 I_2$ for GGIW implementations, and it is uniformly distributed in the entire region for particle-based implementations. In addition, for particle-based implementations, the proposal distribution for the kinematic state is given by its motion model, whereas for the extent matrix its proposal is given by a mean-preserving Wishart distribution with degree of freedom 10000, and for the measurement rate its proposal is given by a mean-preserving gamma distribution with rate parameter 10000. The details of the GGIW prediction can be found in [11].

²The implementation of PMB-PPP-BP is modified based on the MATLAB code at <https://github.com/yuhsuansia/Trajectory-PMB-EOT-BP> to account for an unknown Poisson measurement rate. MATLAB code of PMB(M)-SO-ZIP is available at <https://github.com/yuhsuansia/Extended-target-PMBM-tracker>.

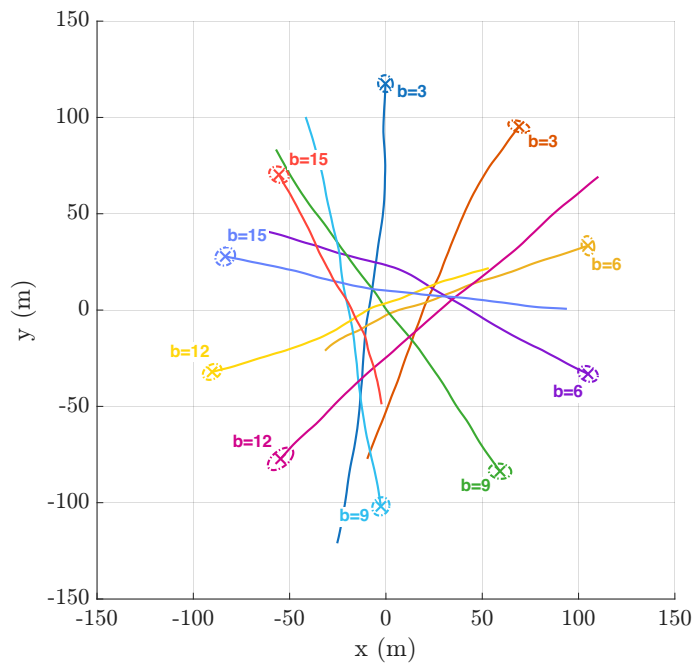


Fig. 2. Illustration of the ground-truth scenario. Two objects are born at each of the time steps 3, 6, 9, 12, and 15, while two objects are dead at time steps 83, 86, 89, 92, and 95. The initial object locations are indicated by crosses, along with their corresponding elliptical extents. Text annotations specify the birth times; e.g., $b = k$ denotes that an object appears at time step k .

TABLE I
MULTI-OBJECT FILTERING PERFORMANCE EVALUATED USING THE GOSPA METRIC, TOGETHER WITH ITS DECOMPOSITION INTO STATE ESTIMATION, MISSED DETECTION, AND FALSE DETECTION ERRORS, AS WELL AS RUNTIME (IN SECONDS), AVERAGED OVER 100 TIME STEPS.

	$p^D = 0.9, \gamma = 10$					$p^D = 0.9, \gamma = 5$					$p^D = 0.8, \gamma = 10$				
	Total	State	Miss	False	Runtime	Total	State	Miss	False	Runtime	Total	State	Miss	False	Runtime
PMB-BP-ZIP	7.39	5.32	0.80	1.26	219.5	10.16	7.16	0.70	2.29	119.1	8.80	5.68	0.81	2.31	197.1
PMB-BP-PPP	63.39	10.88	6.62	45.89	374.1	13.36	7.47	3.59	2.29	118.6	62.81	12.90	12.78	37.13	325.3
PMBM-SO-ZIP	7.76	5.34	1.51	0.90	576.2	9.76	7.20	1.08	1.49	324.5	8.92	5.67	1.49	1.76	544.9
PMB-SO-ZIP	9.90	5.19	3.81	0.91	354.3	11.94	6.95	2.96	1.03	173.1	11.46	5.41	4.33	1.72	320.1

As for the measurement model, the single measurement likelihood is Gaussian with $\ell_k(z|x_k) = \mathcal{N}(z; He_k, E_k)$, $H = I_2 \otimes [1 \ 0]$. The object detection probability is p^D , and the Poisson object measurement rate is γ . In the simulation, we consider three different settings with $(p^D, \gamma) \in \{(0.9, 10), (0.9, 5), (0.8, 10)\}$. The Poisson clutter measurements are uniformly distributed in the region of interest with rate $\lambda^C = 10$. Since PMB-BP-PPP assumes $p^D = 1$, we set the parameter γ used in PMB-BP-PPP to be $p^D\gamma$ for a fair comparison.

For PMB-BP-ZIP and PMB-BP-PPP, the number of particles is 5000 with systematic resampling applied at every time step, and the number of iterations for loopy BP is 3. In addition, we use message censoring and measurement reordering to facilitate track initialization and also adopt measurement-driven initialization for newly detected objects [26]. We also discard Bernoulli components with existence probability smaller than 10^{-3} . For PMBM-SO-ZIP and PMB-SO-ZIP, the pruning thresholds for global hypotheses, GGIW components in the Poisson intensity for undetected objects and Bernoulli components are set to 10^{-2} , 10^{-3} and 10^{-3} , respectively. We also apply ellipsoidal gating with a gate size 13.8. The number of sampling iterations for data association is set to $\lceil 100m_k w_a \rceil$ for global hypothesis with weight w_a in PMBM-SO-ZIP and $50m_k$ in PMB-SO-ZIP.

To extract object state estimates from the filtering density, for all the filters, we apply a threshold of 0.5 on the existence probabilities of Bernoulli components. As for PMBM-SO-ZIP, since it maintains multiple global hypotheses, we first select the global hypothesis with the highest weight and then extract estimates from its Bernoulli components. The performance is evaluated using the generalized optimal subpattern assignment (GOSPA) metric [29] with $\alpha = 2$, exponent $p = 1$, cut-off $c = 20$. The base measure used in GOSPA is the square root Gaussian Wasserstein distance for comparing two extended object states with elliptical shapes [30].

Table I summarizes the performance of the different filters in terms of GOSPA error, its decomposition into state estimation, missed detection, and false detection errors, as well as runtime. The results show that PMB-BP-ZIP achieves in general the best performance in terms of GOSPA across all three settings. In particular, PMB-BP-ZIP significantly outperforms PMB-BP-

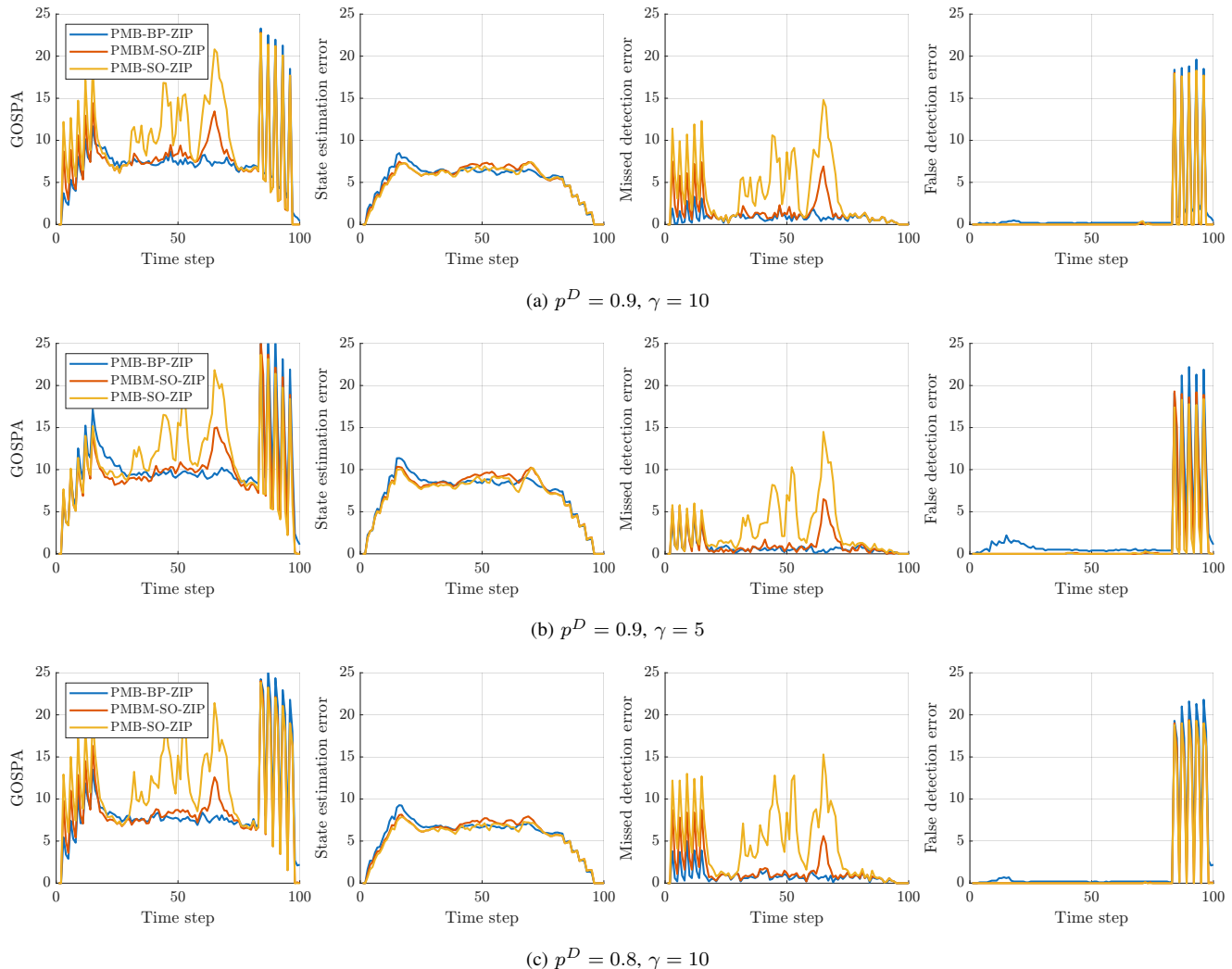


Fig. 3. Performance comparison of PMB-BP-ZIP, PMBM-SO-ZIP and PMB-SO-ZIP, showing the GOSPA error and its decomposition over time.

PPP, which performs poorly due to measurement model mismatch, especially in the case of higher Poisson measurement rate. Compared to PMBM-SO-ZIP and PMB-SO-ZIP, PMB-BP-ZIP has lower GOSPA error in two out of three settings, and it has a significantly lower missed detection error than both PMBM-SO-ZIP and PMB-SO-ZIP across all three settings. In addition, PMB-BP-ZIP has a significantly lower runtime than PMBM-SO-ZIP, but a higher runtime than PMB-SO-ZIP.

We also note that the differences in GOSPA errors between PMB-BP-ZIP and PMBM-SO-ZIP are less pronounced than those reported in [17] for a similar scenario but with the Poisson object measurement model. This may be attributed to the fact that, the ZIP measurement model introduces additional cycles in the factor graph, which can degrade the accuracy of the loopy BP approximation.

To further analyze the filtering performance of PMB-BP-ZIP, PMBM-SO-ZIP, and PMB-SO-ZIP, Fig. 3 presents the GOSPA error and its decomposition over time for the three scenario settings. It can be observed that PMB-BP-ZIP yields a substantially lower missed detection error than both PMBM-SO-ZIP and PMB-SO-ZIP across all three settings, especially at the time steps when objects are born and when closely-spaced objects become separated. The superior track initialization performance of PMB-BP-ZIP might be attributed to its measurement-driven proposal distribution for new Bernoulli components, although this comes at the cost of increased sensitivity to false detections. We also note that, although both PMB-BP-ZIP and PMB-SO-ZIP employ an MB approximation, only PMB-SO-ZIP suffers from coalescence, while PMB-BP-ZIP performs significantly better when objects are moving in proximity. This advantage stems from its particle-based state representation, which can better capture posterior multi-modality than the parametric representation adopted in PMBM-SO-ZIP and PMB-SO-ZIP.

VII. CONCLUSIONS

In this paper, we have presented an extended object PMB filter under the ZIP object measurement model and its implementation using particle BP. This is derived by applying loopy BP to the factor graph representation of the joint factorized

posterior over set of objects, object detection variables, and dual representation of measurement-oriented and object-oriented data association variables. The results show that the proposed filter achieves better performance compared to the extended object PMBM filter using sampling-based method in terms of estimation error and runtime. Interesting future research directions include the extension to sets of trajectories to enable principled object trajectory estimation [17], [24], [25], the development of BP-based implementations for more general object and clutter measurement models [13], [14], the combination with mean-field variational inference to further reduce the computational complexity [31], and the extension to multi-sensor fusion and multi-scan smoothing [32] using set-type BP [33].

REFERENCES

- [1] Y. Bar-Shalom, P. K. Willett, and X. Tian, *Tracking and data fusion*. YBS publishing Storrs, CT, USA:, 2011, vol. 11.
- [2] K. Granström, M. Baum, and S. Reuter, "Extended object tracking: Introduction, overview and applications," *Journal of Advances in Information Fusion*, vol. 12, no. 2, 2017.
- [3] K. Gilholm and D. Salmund, "Spatial distribution model for tracking extended objects," *IEE Proceedings-Radar, Sonar and Navigation*, vol. 152, no. 5, pp. 364–371, 2005.
- [4] S. P. Coraluppi and C. A. Carthel, "Multiple-hypothesis tracking for targets producing multiple measurements," *IEEE Transactions on Aerospace and Electronic Systems*, vol. 54, no. 3, pp. 1485–1498, 2018.
- [5] X. Tang, M. Li, R. Tharmarasa, and T. Kirubarajan, "Seamless tracking of apparent point and extended targets using Gaussian process PMHT," *IEEE Transactions on Signal Processing*, vol. 67, no. 18, pp. 4825–4838, 2019.
- [6] G. Vivone and P. Braca, "Joint probabilistic data association tracker for extended target tracking applied to X-band marine radar data," *IEEE Journal of Oceanic Engineering*, vol. 41, no. 4, pp. 1007–1019, 2016.
- [7] S. Yang, K. Thormann, and M. Baum, "Linear-time joint probabilistic data association for multiple extended object tracking," in *10th Sensor Array and Multichannel Signal Processing Workshop*. IEEE, 2018, pp. 6–10.
- [8] K. Granström, C. Lundquist, and O. Orguner, "Extended target tracking using a Gaussian-mixture PHD filter," *IEEE Transactions on Aerospace and Electronic Systems*, vol. 48, no. 4, pp. 3268–3286, 2012.
- [9] C. Lundquist, K. Granström, and U. Orguner, "An extended target CPHD filter and a gamma Gaussian inverse Wishart implementation," *IEEE Journal of Selected Topics in Signal Processing*, vol. 7, no. 3, pp. 472–483, 2013.
- [10] M. Beard, S. Reuter, K. Granström, B.-T. Vo, B.-N. Vo, and A. Scheel, "Multiple extended target tracking with labeled random finite sets," *IEEE Transactions on Signal Processing*, vol. 64, no. 7, pp. 1638–1653, 2016.
- [11] K. Granström, M. Fatemi, and L. Svensson, "Poisson multi-Bernoulli mixture conjugate prior for multiple extended target filtering," *IEEE Transactions on Aerospace and Electronic Systems*, vol. 56, no. 1, pp. 208–225, 2020.
- [12] Y. Xia, K. Granström, L. Svensson, M. Fatemi, Á. F. García-Fernández, and J. L. Williams, "Poisson multi-Bernoulli approximations for multiple extended object filtering," *IEEE Transactions on Aerospace and Electronic Systems*, vol. 58, no. 2, pp. 890–906, 2022.
- [13] Á. F. García-Fernández, J. L. Williams, L. Svensson, and Y. Xia, "A Poisson multi-Bernoulli mixture filter for coexisting point and extended targets," *IEEE Transactions on Signal Processing*, vol. 69, pp. 2600–2610, 2021.
- [14] Á. F. García-Fernández, Y. Xia, and L. Svensson, "Poisson multi-Bernoulli mixture filter with general target-generated measurements and arbitrary clutter," *IEEE Transactions on Signal Processing*, vol. 71, pp. 1895–1906, 2023.
- [15] Á. F. García-Fernández, J. L. Williams, K. Granström, and L. Svensson, "Poisson multi-Bernoulli mixture filter: direct derivation and implementation," *IEEE Transactions on Aerospace and Electronic Systems*, vol. 54, no. 4, pp. 1883–1901, 2018.
- [16] J. L. Williams, "Marginal multi-Bernoulli filters: RFS derivation of MHT, JIPDA, and association-based member," *IEEE Transactions on Aerospace and Electronic Systems*, vol. 51, no. 3, pp. 1664–1687, 2015.
- [17] Y. Xia, Á. F. García-Fernández, F. Meyer, J. L. Williams, K. Granström, and L. Svensson, "Trajectory PMB filters for extended object tracking using belief propagation," *IEEE Transactions on Aerospace and Electronic Systems*, vol. 59, no. 6, pp. 9312–9331, 2023.
- [18] K. Granström, L. Svensson, S. Reuter, Y. Xia, and M. Fatemi, "Likelihood-based data association for extended object tracking using sampling methods," *IEEE Transactions on Intelligent Vehicles*, vol. 3, no. 1, pp. 30–45, 2018.
- [19] F. Meyer and J. Williams, "Scalable detection and tracking of geometric extended objects," *IEEE Transactions on Signal Processing*, vol. 69, no. 6283–6298, 2021.
- [20] Y. Li, P. Wei, Y. Wei, L. Gao, and H. Zhang, "Loopy sum-product algorithm based joint detection, tracking and classification of extended objects with analytic implementations," *Signal Processing*, vol. 196, p. 108520, 2022.
- [21] Y. Li, T. Shen, and L. Gao, "Multisensor multiple extended objects tracking based on the message passing," *IEEE Sensors Journal*, vol. 24, no. 10, pp. 16 510–16 528, 2024.
- [22] R. Lyu, L. Hao, L. Zheng, and Y. Cai, "A fast Poisson labeled multi-Bernoulli filter for extended object tracking using belief propagation," *Signal Processing*, vol. 238, p. 110156, 2026.
- [23] W. Ma, Z. Jing, P. Dong, and H. Leung, "Max sum based data associations for tracking point and extended targets," *IEEE Transactions on Aerospace and Electronic Systems*, vol. 61, no. 2, pp. 3059–3075, 2025.
- [24] Á. F. García-Fernández, L. Svensson, J. L. Williams, Y. Xia, and K. Granström, "Trajectory Poisson multi-Bernoulli filters," *IEEE Transactions on Signal Processing*, vol. 68, pp. 4933–4945, 2020.
- [25] K. Granström, L. Svensson, Y. Xia, J. Williams, and Á. F. García-Fernández, "Poisson multi-Bernoulli mixtures for sets of trajectories," *IEEE Transactions on Aerospace and Electronic Systems*, vol. 61, no. 2, pp. 5178–5194, 2024.
- [26] F. Meyer and J. L. Williams, "Scalable detection and tracking of extended objects," in *International Conference on Acoustics, Speech and Signal Processing*. IEEE, 2020, pp. 8916–8920.
- [27] M. S. Arulampalam, S. Maskell, N. Gordon, and T. Clapp, "A tutorial on particle filters for online nonlinear/non-Gaussian Bayesian tracking," *IEEE Transactions on Signal Processing*, vol. 50, no. 2, pp. 174–188, 2002.
- [28] M. Feldmann, D. Franken, and W. Koch, "Tracking of extended objects and group targets using random matrices," *IEEE Transactions on Signal Processing*, vol. 59, no. 4, pp. 1409–1420, 2011.
- [29] A. S. Rahmathullah, Á. F. García-Fernández, and L. Svensson, "Generalized optimal sub-pattern assignment metric," in *Proceedings of International Conference on Information Fusion*. IEEE, 2017, pp. 1–8.
- [30] S. Yang, M. Baum, and K. Granström, "Metrics for performance evaluation of elliptic extended object tracking methods," in *International Conference on Multisensor Fusion and Integration for Intelligent Systems*. IEEE, 2016, pp. 523–528.
- [31] W. Ma, Z. Jing, P. Dong, and H. Leung, "Closed-form message passing algorithms for tracking extended targets," *IEEE Transactions on Aerospace and Electronic Systems*, vol. 62, pp. 5084–5101, 2026.
- [32] J. L. Williams and R. A. Lau, "Multiple scan data association by convex variational inference," *IEEE Transactions on Signal Processing*, vol. 66, no. 8, pp. 2112–2127, 2018.
- [33] H. Kim, Á. F. García-Fernández, Y. Ge, Y. Xia, L. Svensson, and H. Wymeersch, "Set-type belief propagation with applications to Poisson multi-Bernoulli SLAM," *IEEE Transactions on Signal Processing*, vol. 72, pp. 1989–2005, 2024.